Validating Magnetopause Models using Cluster Observations

Samuel John Brian Lewis

A dissertation submitted for the degree of
Master of Science in Physics

Physics Department
Lancaster University

May, 2026

Validating Magnetopause Models using Cluster Observations

Samuel John Brian Lewis
Physics Department, Lancaster University

A dissertation submitted for the degree of *Master of Science* in Physics.

May, 2026

Abstract

Earth's magnetosphere protects the terrestrial atmosphere from the solar wind and the interplanetary magnetic field. The magnetopause is the boundary between the magnetosheath and the magnetosphere, acting as the edge of the region of space dominated by Earth's magnetic field and plasma. Therefore, the location and geometry of the magnetopause are important properties to understand in order to facilitate better planning for satellite investigations within this region, and to reveal the natural process underpinning space weather. Using the Cluster mission, this dissertation investigates the size and shape of Earth's magnetopause, to test the validity of current magnetopause models. It is found that the Cluster data and the models agree with at most a 15% disagreement over all latitudes and local times. The greatest disagreement between models arises with the magnetospheric cusp region as this feature is not included in the cylindrically symmetric Shue *et al.* (1998) model, but is included in the asymmetric Lin *et al.* (2010) and Liu *et al.* (2015) models; models that are relatively simple to compute in comparison to other magnetopause models that include this cusp region. The validity of the newly introduced Geospace Region and Magnetospheric Boundary dataset (GRMB), developed by Grison *et al.* (2025), has been briefly tested. This proves a useful resource for identifying the region Cluster is in. However, this database includes some inaccurate magnetopause crossings, featuring spatial ambiguities up to 15 Earth Radii for some cases. Overall, this dissertation confirms that the GRMB database can be a useful resource provided caution is used with some identified regions, and that some of the currently used magnetopause models are broadly accurate with some drawbacks in certain regions, although this is dependant on the precision required.

Acknowledgements

I would like to thank my supervisor Jim for supporting and guiding me through this project. Thanks to Lana for reading and checking my final version of this dissertation. I would like to thank the Space and Planetary Physics group at Lancaster University for including me within the group, and their helpful suggestions with my work. I would especially like to thank Melissa for supporting me every step during the entire process of this project and reading many stages of the dissertation. I would also like to thank my family for supporting me not only with this project, but also my journey to this stage of my education.

Contents

Chapter 1

Introduction

The Cluster spacecraft has been vital in analysing many structures within the space plasma environment. With the introduction of the GRMB dataset by Grison *et al.* (2025), this analysis has become significantly easier, as the region the Cluster spacecraft are in is already identified. This dissertation focuses on the magnetopause: the size and shape that Cluster observes. This size and shape is then compared to magnetopause models, both cylindrically symmetric and asymmetric, to confirm the validity and precision of the models. The usability of the GRMB dataset is also tested within this dissertation.

1.1 Theory and Background

The solar wind is a stream of charged particles that becomes gravitationally unbound from the rest of the solar corona, due to heating (e.g. Chandran *et al.*, 2025). The mechanism that heats the solar corona to 1,000,000K is still an open question in solar physics. Some of the heating mechanisms that are theorised to be responsible include the stressing of coronal magnetic fields, or through convective motion of solar plasma causing disturbances that travel into the corona, explored in Doorsselaere *et al.* (2020). The particles that make up the solar wind are primarily protons and electrons, with some Helium nuclei. The solar wind can be found with varying speeds and densities dependant on which type of solar wind is present: slow or fast solar wind. Slow solar wind travels at a speed between 300-500 kms^{-1} and number densities around 10 cm^{-3}; fast solar wind travels between 700-800 kms^{-1} with number densities around 3 cm^{-3} (e.g. Chandran *et al.*, 2025).

The Interplanetary Magnetic Field (IMF) is then a result of solar wind, where the Sun's magnetic field gets carried out by the solar wind particles. This then propagates through the solar system in a spiral pattern, called a Parker spiral. The spiral effect is caused by the angular momentum of the Sun, as the particles will be emitted radially from the surface of the Sun, which when combined with other particles emitted at different points in time

creates a curved magnetic field line. When several of these magnetic field lines are taken into account, a spiral effect is observed (e.g. Owens and Forsyth, 2013).

A plasma is a collection of either partially or fully ionised particles. Different compositions of plasma can be found within and surrounding Earth's magnetosphere. They will interact with any magnetic or electrical field via the Lorentz force, shown in equation 1.1.

$$\mathbf{F} = q\left(\mathbf{E} + \mathbf{v} \times \mathbf{B}\right) \tag{1.1}$$

Equation 1.1 shows that a force $\mathbf{F}$ will be applied to any charged particle moving through an electric field $\mathbf{E}$ or magnetic field $\mathbf{B}$, with velocity $\mathbf{v}$ and charge q.

1.1.1 Magnetosphere

A magnetosphere is the region around a planet where the environment is dominated by the planet's magnetic field, whether intrinsic or induced by the IMF and solar wind. Earth's magnetic field is generated from the movement within the iron outer core, i.e. intrinsic to the planet. This causes the magnetosphere to be much larger than an induced magnetosphere that you might find at a planet such as Mars. However, because of the size of Earth and its core, the magnetosphere is much smaller than Jupiter's magnetosphere, the largest object in the solar system. The size of the magnetosphere will be heavily influenced by the solar wind conditions, as the magnetosphere will be compressed more with a stronger solar wind pressure, for example.

The early concepts of the magnetosphere originate with Chapman and Ferraro (1931a and 1931b). This article was an investigation into the causes of geomagnetic storms: periods of high solar wind intensity, with high velocity or density. This is a result of larger solar activity and can cause periods of extreme geomagnetic activity, resulting in many space weather effects. Chapman and Ferraro theorised that a stream of particles will be emitted from the Sun in a given area. These streams follow the Parker spiral curve, explained in the previous section and seen in figure 1.1. When approaching Earth, this stream of particles will have a magnetic force applied to it. This will slow the stream, allowing compression between streams, when more particle streams are considered. This magnetic force is based on the velocity ($\mathbf{v}_n$) and the distance from Earth (r), shown in equation 1.2.

$$\textbf{Force} \propto \frac{\mathbf{v}_n}{r^6} \tag{1.2}$$

With the streams of particles permeating through all of space, and the magnetic force influenced by the distance to Earth; there will be a region around Earth where the particles are slowed. This creates a region surrounding Earth where no solar wind is present, which

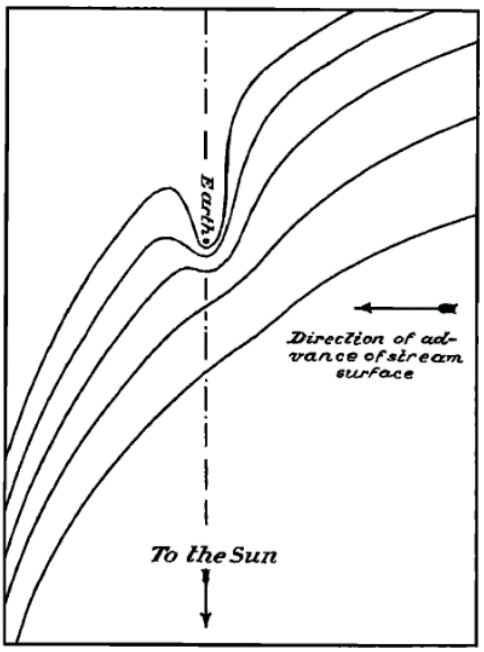

Figure 1.1: Figure 2 in Chapman and Ferraro (1931b): A representation of how streams of particles interact with Earth. Each stream of particles is represented with one line, showing their progression. These streams get compressed as they approach Earth, causing them to bend around Earth, a result of the magnetic force expressed in equation 1.2

will eventually become known as the magnetosphere. The effect described is shown in figure 1.1: this is figure 2 in Chapman and Ferraro (1931b).

The dipole found at Earth is then included in their considerations. This was done by first considering the field of a "doublet": which emerges as field lines centred around two points (representing the poles of Earth's magnetic field), with a high magnetic field strength between the two centres. This "doublet" is then introduced to an infinitely conductive plane, which will compress one side of the magnetic field. This results in a stronger magnetic field on that side, with the compression of magnetic field lines. This will also result in weaker field strength associated with open magnetic field lines created by the introduction of this plane. These regions were assumed to not affect the shape of the magnetosphere once the model was formed, but are in fact the field lines associated with the magnetospheric cusp regions. This conductive plane then progresses past the magnetic field centres to give the shape represented in figure 1.2: this is figure 5 in Chapman and Ferraro (1931b).

The magnetospheric cusp region is defined as the point where dayside (Sun facing side of the Earth) and nightside (opposite to the Sun facing side of the Earth) magnetic field lines

converge towards the geomagnetic poles (e.g. Pitout and Bogdanova, 2021). This emerges as a funnel shaped region located beyond Earth's magnetic poles. This is a region of weaker magnetic force from Earth's magnetic field, due to diverging magnetic field lines, causing the solar wind to compress the magnetosphere further in this region. This causes an indentation in the magnetopause, when compared to the cylindrically symmetric shape that a number of models take.

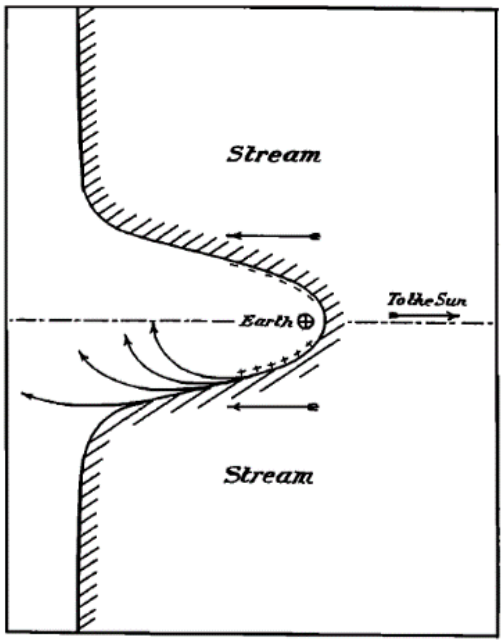

Figure 1.2: Figure 5 in Chapman and Ferraro (1931b): Chapman and Ferraro's interpretation of the magnetosphere. This is produced by moving an infinitely conductive plane over a magnetic dipole

After the magnetosphere had been first theorised by Chapman and Ferraro (1931), it took until the Explorer 12 spacecraft before the first in-situ observations were taken of the magnetopause. This was reported by Cahill and Amazeen (1963), where the data from Explorer 12's magnetometer was analysed for between 16 August to 30 September 1961, in which nine magnetopause crossings were found. They found the magnetopause at 10 to $11R_E$ (Earth radii), near the Earth-Sun line, for magnetically calm periods. There was a variable thickness of boundary observed of between 100 km and 1000 km. There also seemed to be twice the strength of magnetic field just within the magnetopause, then what had been predicted up to that point.

This was then expanded upon with the use of data from IMP 1-4, Explorer 33 and 35

in Fairfield (1971). Here both the magnetopause and bow shock locations detected from these spacecraft were analysed and compared to a previous model, by Olson (1969) for the magnetopause. Fairfield found the magnetopause to be $11R_E$ in the sunward direction, $16.1R_E$ in the dawn meridian and $15.8R_E$ in the dusk meridian. Figure 1.3 taken from Fairfield (1971), represents previous studies of the magnetopause.

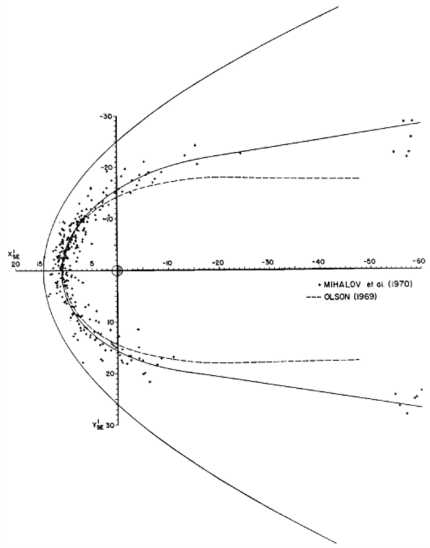

Figure 1.3: Figure 2 in Fairfield (1971). The Olson (1969) model (dashed-line curve) compared to the best fit of the points from Mihalov *et al.* (1970) that have been rotated 4° to account for the solar wind aberration. The solid outer line is the best fit for the bow shock found in figure 1 in Fairfield (1971). Shown in solar ecliptic (SE) coordinates, in the X-Y plane

The magnetospheric cusp region seen in Hedgecock and Thomas (1975) can be found between 64° and 66° latitude, shown in figure 1.4. More recent models of the magnetopause take account of this compression when forming the models. With the addition of the tilt in Earth's magnetic dipole, the resulting models will be asymmetrical: the tilt will cause a different interaction with the solar wind as it encounters the magnetic field at an angle.

These findings were then enhanced with the use of the ISEE 1 and 2 spacecraft: the first mission to use multiple spacecraft with a small separation to measure the magnetopause. The use of this mission verified the existence of magnetic reconnection, where magnetic field lines from Earth's magnetic dipole connect with field lines in the solar wind. This was found by Paschmann *et al.* (1979), where they found higher ion and electron flow speeds in the magnetopause, when compared to the magnetosheath and magnetosphere. Reconnection occurs when the magnetic field lines are in anti-parallel directions (when there is southward IMF) and will cause an X-shaped transition region, where plasma is transferred across the

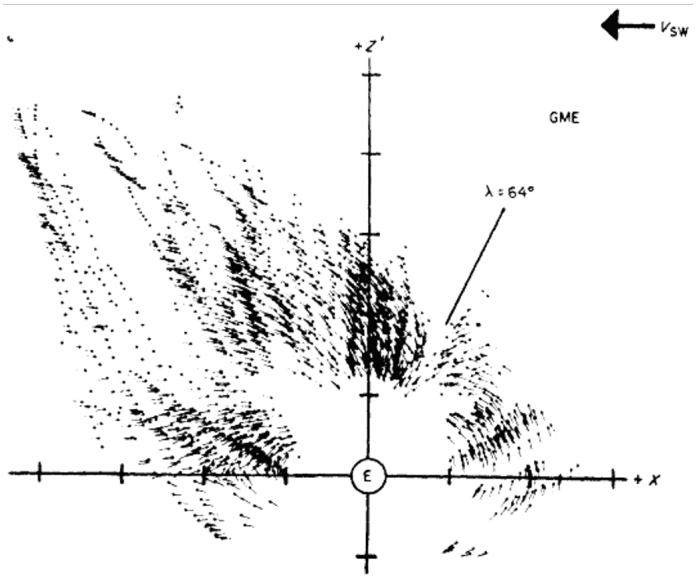

Figure 1.4: Figure 3 in Hedgecock and Thomas (1975). Measurements of the magnetic field directions surrounding Earth using data from the HEOS-1 and HEOS-2 satellites. This is using geocentric magnetospheric equatorial (GME) coordinates. The magnetospheric cusp region can be seen at 64^o latitude

magnetopause into the magnetosphere. The magnetopause will be compressed during periods of reconnection due to a reduction in magnetic pressure from Earth's magnetic field, therefore, it is highly important to the structure of the magnetopause.

The investigations into the ISEE data didn't stop with reconnection, with refined thickness and location of the magnetopause found by Berchem and Russell (1982a). They found that the magnetopause is characteristically between 400 and 1000 km thick, and can commonly be found at larger thicknesses. They also found that the thickness of the magnetopause is not dependant on the orientation of the magnetosheath magnetic field. There was also a constant rapid irregular motion exhibited by the magnetopause with speeds commonly between $10\,\mathrm{kms}^{-1}$ and $80\,\mathrm{kms}^{-1}$.

In Sibeck *et al.* (1991) the extent of the solar wind conditions affecting the magnetopause position had started to be considered. They used data from a variety of missions such as the IMP, Explorer, ISEE and Prognoz missions and found that the dynamic pressure and IMF B_z (Z component of the magnetic field strength of the solar wind) parameters of the solar wind are important to the structure of the magnetopause. An analysis of the difference between northward and southward IMF B_z was also undertaken, where a higher compression of the magnetopause was measured for southward IMF B_z. These two parameters then became the

basis of the Shue *et al.* (1998) model. The Shue model is studied within this investigation as it is widely used, and an older model; introduced further in section 2.5.1.

Further observations were taken by the Equator-S spacecraft between December 1997 and March 1998. These observations were focussed on the dayside magnetopause, between local times 6:00 and 10:40. Local time represents the relative position to the Sun of a particular point around a planet, using 24 hours as a full rotation, starting at midnight the opposite side to the Sun. Shown in Dunlop *et al.* (1999), the Equator-s orbit had an apogee of around 10.6 R_E, at which point the spacecraft was just outside the magnetopause in most cases. This suggests the magnetopause will be found in this region commonly, supporting the idea of a dayside magnetopause at around the 10 to 11R_E point.

Soon after the Cluster spacecraft was launched, representing the next significant jump in magnetopause measurements. This mission has allowed confirmation of the location and velocities of the magnetopause taken by previous spacecraft. Cluster also gave further insight into the internal structures of the magnetopause. This was achieved by using observations from all four spacecraft together, to analyse changes in the magnetopause with the spacecraft travelling through at slightly different times. In addition, the magnetospheric cusps were studied further with the use of Cluster, as higher latitudes were explored than many other spacecraft sent to study the magnetic environment surrounding Earth. This can be seen with Cargill *et al.* (2005), where the cusp region was found to be between 73° and 80° latitude and 10:30 and 13:30 local time. The Cluster mission and spacecraft have been described further in section 2.2. Science results from Cluster have guided the development of more recent missions, such as MMS with the purpose of investigating magnetic reconnection.

Figure 1.5 is a modern interpretation of the magnetosphere, which includes several regions determined by the conditions of the plasma. These are the solar wind as seen in section 1.1; the bow shock, shock generated when the supermagnetosonic solar wind encounters Earth's magnetic field (e.g. Merka *et al.*, 2005); the magnetosheath, a region of decelerated and deflected solar wind that flows between the magnetopause and bow shock (e.g. Lucek *et al.*, 2005); the magnetopause, a thin surface layer acting as the boundary between the magnetosheath and Earth's magnetic field, considered the outer edge of the magnetosphere (e.g. De Keyser *et al.*, 2005); the plasma mantle, a region just inside the magnetopause, containing plasma similar to that of the magnetosheath, extending from the cusps down the magnetotail, carrying plasma tailward (e.g. Wang *et al.*, 2014); North and South magnetospheric lobes, regions of very low density plasma located between the plasma sheet and mantles (e.g. Coxon *et al.*, 2016); the plasma sheet, region of warm dense plasma ($\sim 10^7\,\mathrm{K}$, $0.1 - 1\,\mathrm{cm}^{-3}$) in the near-Earth nightside region, extending down the magnetotail (e.g. Hill, 1974); the ring current, a region of hot reasonably sparse plasma ($10^7 - 10^9\,\mathrm{K}$), located in between the two radiation belts, forming a current flowing around the Earth (e.g.

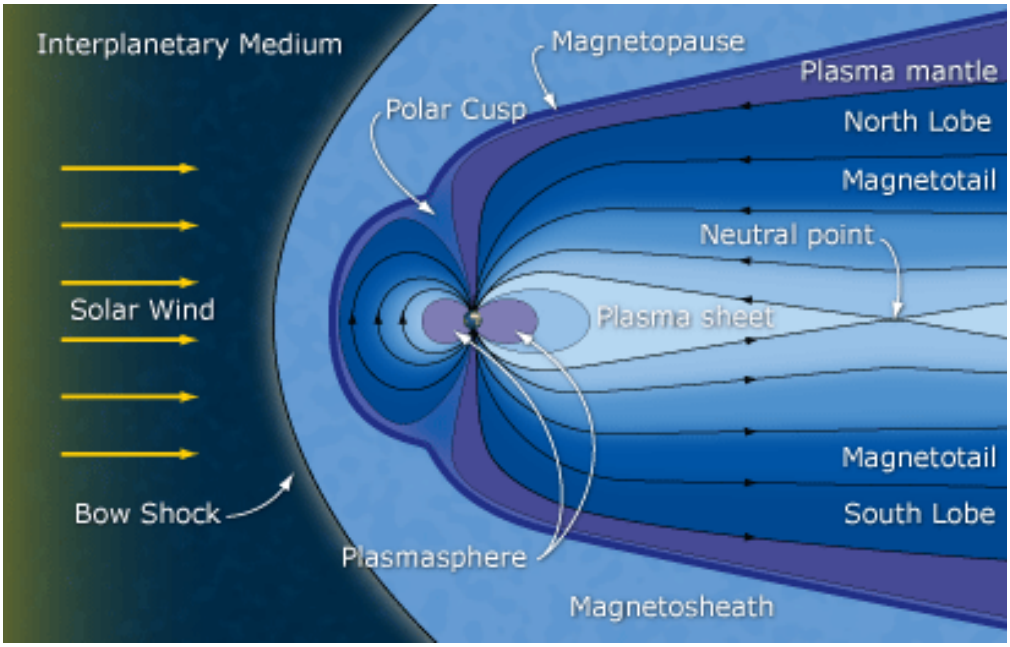

Figure 1.5: Modern interpretation of Earth's magnetosphere. Showing the various plasma regions. The solar wind is represented with yellow arrows. Earth's magnetic field lines are represented by the black arrows (Earth's Magnetic Environment, ESA)

Ferradas *et al.*, 2023); radiation belts, regions of hot sparsely populated plasma ($10^9 - 10^{12}$ K, $< 10^{-6} - 10^{-4}$ cm^{-3}), resulting from cosmic rays and the solar wind plasma, can cause severe problems for satellites if not properly accounted for, as it is primarily made of high energy electrons (e.g. Hands *et al.*, 2018); the plasmasphere, the region directly surrounding the atmosphere with cold dense plasma ($\sim 10^4$ K, up to 10^4 cm^{-3}), with a sharp drop in density defining the outer boundary (e.g. Bianco *et al.*, 2023).

As of more recent estimates, the distance to the nose of Earth's magnetopause (stand-off distance) is between 5.2 and 14 R_E (typically around 10R_E) dependant on the solar wind conditions (Lin et al., 2010). The magnetosphere will then expand further out from Earth down the path of the solar wind. This continues into the magnetotail where the magnetosphere cavity can be found beyond 200 Re from Earth (e.g. Berchem et al., 1998; Sibeck and Lin, 2014). Many models of the magnetopause have been cylindrically symmetric, about the Earth-Sun line. However, this ignores some aspects seen with the magnetopause shape such as the magnetospheric cusp region or the effect seen with the tail current sheet.

In addition to the magnetic dipole, Earth's magnetosphere is driven by currents found within (e.g. Ganushkina *et al.*, 2018). These are flows of electric charge, facilitated by the flow of

plasma through the magnetosphere, which emerge through a number of current patterns. The first pattern relevant to the magnetopause to be discovered were the Chapman-Ferraro currents, suggested in Chapman and Ferraro (1933). These take the form of two ring shapped currents mapping to the magnetopause, surrounding the poles of Earth's magnetic field. This can be seen in figure 1.6, panel A. The second of the current systems takes the form of a thin sheet of current flowing in the magnetotail, starting on the dusk side of the magnetosphere along the equatorial plane (e.g. Ganushkina *et al.*, 2018). This current then flows from the dusk side, around the magnetopause to the dawn side. It then cuts through the centre of the magnetotail to return back to the dusk side via the return current. This will flow both North and South with a magnetic field in both directions. The structure can be seen in figure 1.6, panel B. The final currents relevant to the magnetopause are the field aligned currents. These are magnetospheric currents that flow parallel to Earth's magnetic field lines, and exist in two regions (e.g. Ganushkina *et al.*, 2018). The structure of the field aligned currents can be seen in figure 1.6, panel C.

This dissertation attempts to analyse the effectiveness of magnetopause models including the Shue *et al.* (1998), Lin *et al.* (2010) and Liu *et al.* (2015) models. To do this, the newly published Geospace Region and Magnetospheric Boundary identification dataset is used, developed by Grison *et al.* (2025), for the easier identification of magnetopause crossings. The effectiveness of this new dataset is also analysed to see how useful it might be to identify the region the Cluster spacecraft were in at specific points in time.

1.1.2 Questions About the Magnetosphere

There are still many research questions relating to the magnetopause. For Keyser *et al.* (2005), one of these question includes "By which process can magnetosheath plasma manage to penetrate into the magnetosphere that deeply?" This relates to the plasma entering in to the magnetosphere through reconnection at the magnetopause, and highlights important physics to be discovered in how reconnection events can occur. Questions relating to reconnection are sill being studied, outlined in Borovsky *et al.* (2020), with "What determines when and where reconnection occurs? Under what conditions does it start? What causes it to stop?" A number of causes for reconnection at the magnetopause are known, however, there are fewer reconnection events observed then would be predicted with these factors. This indicates there are other factors that limit the occurrence of reconnection events. The process in which reconnection stops is still not fully understood: some theories include, changing of the properties of the inflow plasma, or that the "plasma somehow gains an unfavourable geometry for reconnection". None of these theories fully explain how reconnection is stopped, and is an important aspect to study as it will explain the ending of substorm reconnection. These questions will be relevant to the structure of the magnetopause as reconnection events result in a compression of the magnetopause, and affect the current systems found there.

A better understanding of the magnetopause structure can provide insight into large-scale magnetospheric drivers.

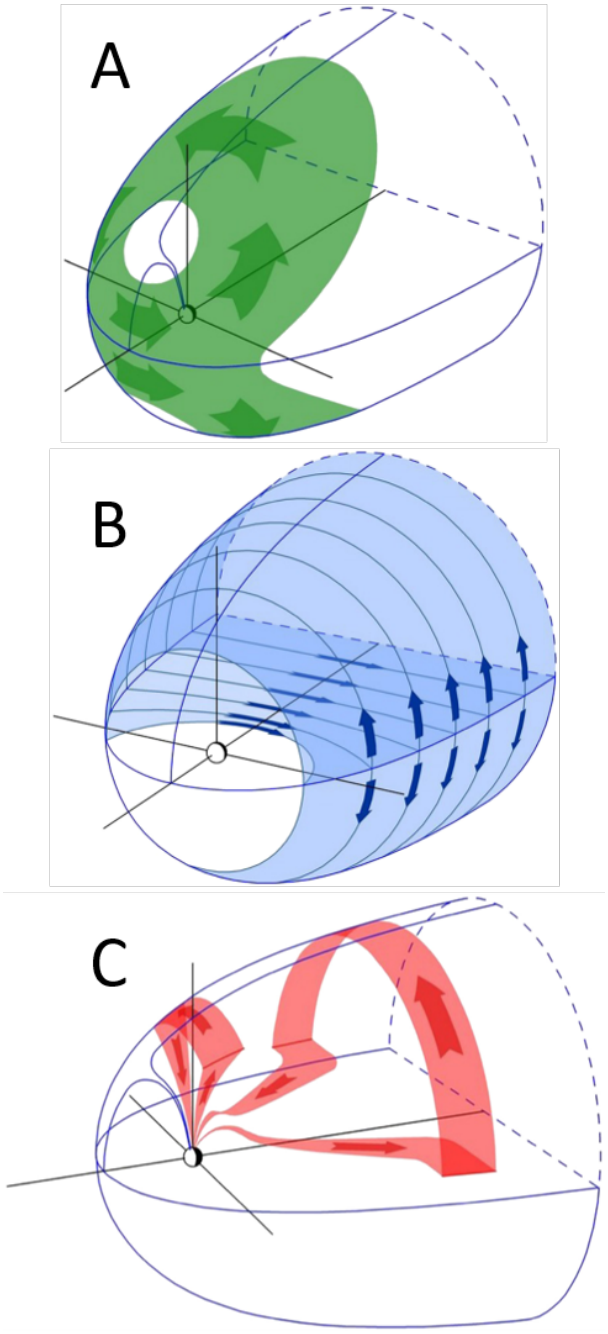

Figure 1.6: Diagram of magnetospheric currents present on the magnetopause, adapted from Ganushkina *et al.* (2018). Panel A represents the Chapman and Ferraro currents, that produce a ring around Earth's magnetic poles on the magnetopause. Panel B represents the cross tail currents, present through the magnetotail, with the return current in the centre. Panel C represents the field aligned currents

Chapter 2

Data and Methodology

2.1 Coordinate Systems

Before any analysis of magnetopause models or spacecraft locations can be done, the reference frame has to be defined. Here the coordinate systems used throughout the analysis are defined.

2.1.1 Geocentric Solar Ecliptic

Geocentric Solar Ecliptic (GSE) is a geocentric-based coordinate system (Earth as the centre of the coordinates). The X axis is along the Sun-Earth line with positive X pointed towards the Sun; the Y axis is in the ecliptic plane (the plane that Earth orbits in) with positive Y opposing Earth's orbital motion; the Z axis is 90° to the other two axis with positive Z pointed north from the ecliptic plane. This produces a reference frame that is easy to understand as there are no moving axis, that is centred on Earth. GSE coordinates allows for a typical orbital path as seen later in figure 2.3 in section 2.2.2.

2.1.2 Geocentric Solar Magnetic

Geocentric Solar Magnetic (GSM) coordinates vary dependant on Earth's magnetic field. The X axis points from the centre of the Earth to the Sun; the Y axis is perpendicular to Earth's magnetic dipole axis and the Earth-Sun line, positive Y opposing Earth's orbital motion; the Z axis is in the plane of the dipole axis and Earth-Sun line, positive Z directed northward (e.g. Laundal and Richmond, 2017). Therefore, GSE and GSM coordinates have the same X axis, but different Y and Z axes, which can be seen in figure 2.1. Overall, within GSE coordinates Earth's dipole axis moves in all three dimensions, while in GSM coordinates it moves in two dimensions contained in the X-Z plane (e.g. Laundal and Richmond, 2017). This gives a much better representation of the magnetosphere in terms of the magnetic field,

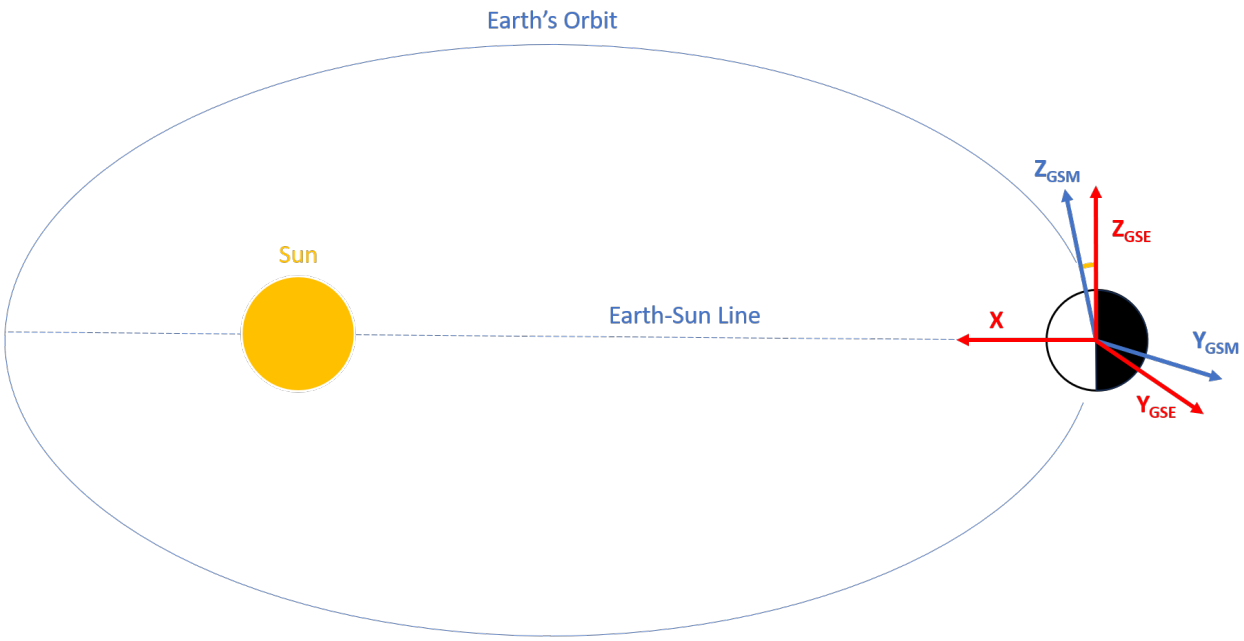

Figure 2.1: Diagram showing the GSE and GSM coordinate systems. The Earth is shown as the black and white circle, the white representing the dayside and the black representing the nightside. GSE coordinates are shown in red, GSM coordinates are shown in blue except for the X axis which GSE and GSM coordinates share

instead of the relative position fixed to Earth's orientation compared to the Sun. This leads to a slight difference in some of the comparison graphs.

2.2 Cluster

The European Space Agency (ESA) Cluster mission was first proposed in 1982, as a mission investigating small-scale structures and macroscopic turbulences in the magnetosphere (e.g. Escoubet *et al.*, 2021). This proposal was developed as four identical spacecraft set to launch in June 1996 on the maiden launch of the Ariane 5 rocket. However, this was ill-fated, as 30 seconds after launch the guidance system onboard Ariane 5 encountered an error (Ariane 501 Inquiry Board Report). This resulted in the loss of the original Cluster spacecraft.

After this loss the Cluster spacecraft were rebuilt and launched onboard two Soyuz rockets in July and August 2000. This again was comprised of four Cluster satellites (two in each rocket), with the science phase starting in February 2001. This phase ended by October 2024, with only two of the satellites still in orbit by December 2025. This creates a complete dataset, spanning approximately 23 years. The main objective was to measure the space

plasma environment surrounding Earth, including the regions of the magnetosphere, the magnetopause, the magnetospheric cusps, the magnetosheath, the bow shock and the IMF. In order to do this, the four satellites were equipped with an identical suite of instruments, described in section 2.2.1. Each of these satellites are cylinders with a height of 1.3 m and a diameter of 2.9 m (e.g. Credland *et al.*, 1997).

The higher latitudes of Earth's magnetosphere are regions less commonly explored by satellites investigating the plasma environment near Earth. These higher latitudes were some of the target regions of the Cluster mission, allowing the measurement the magnetospheric cusp region (Cluster Overview, ESA). Due to orbit degradation, Cluster also explored the lower latitudes, giving a view of most of the magnetosphere, this effect can be seen in figure 2.2. This allows a larger range of latitudes to be considered when determining the location of the magnetopause.

Figure 2.2 shows how Cluster's orbit develops in latitude during the mission. The 2007 and 2012 orbits are more elliptical and are further in the negative Z direction at apogee than the 2017 and 2020 orbits. The 2017 orbit is more circular than the two earlier orbits and has an apogee at a much lower latitude. The 2020 orbit's apogee is slightly in the positive Z direction and has a similar shape to the 2017 orbit. This shows that as Cluster's mission progressed, the obits became more circular and lower in latitude, in the X-Z plane. There also seems to be a bias for the southern hemisphere in the earlier years. This is observed by Förster and Haaland (2015), with the data availability of the EDI instrument (introduced in section 2.2.1) having a slight southern hemisphere bias between the start of the mission and 2010.

In figure 2.2, the two solid black lines represent two boundaries associated with the magnetosphere. The innermost boundary is an average prediction of the magnetopause location using the Roelof and Sibeck (1993) model; the outermost boundary is the average prediction of the magnetosheath boundary. These are included to give an idea of whether Cluster is likely to cross these boundaries, which occurs in figure 2.2 for both boundaries.

2.2.1 Cluster Instruments

Each Cluster Spacecraft is fitted with an identical suite of instruments (Instruments II, ESA), including:

- FluxGate Magnetometer, FGM
  Two magnetometers that measured the magnetic field the spacecraft encountered. One attached to the main spacecraft, one located on a 5 m boom to avoid interference from the spacecraft

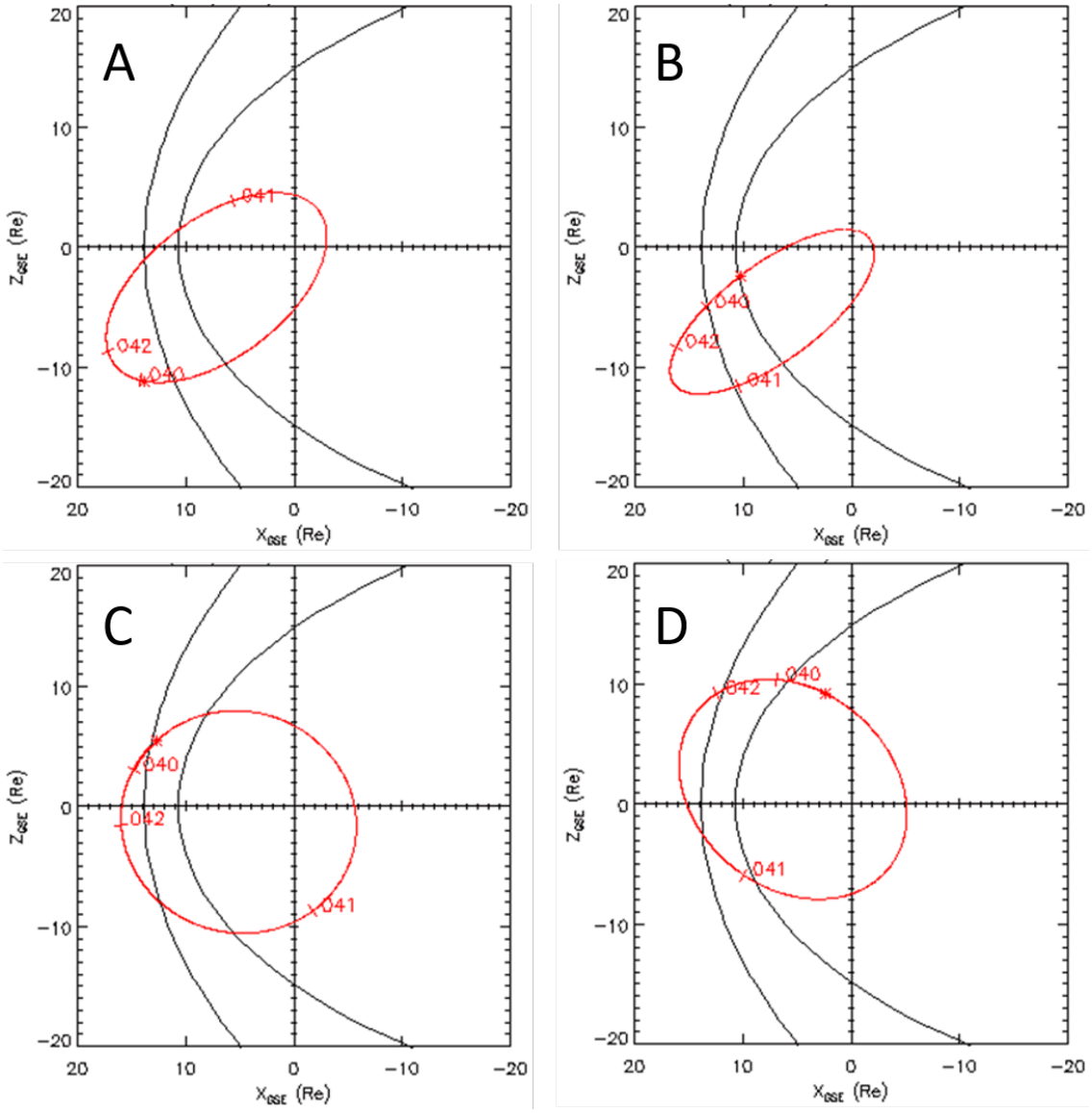

Figure 2.2: The evolution of Cluster's orbit through the mission. This is in the GSE X-Z plane. Panel A is between 09/02/2007 and 11/02/2007. Panel B is between 09/02/2012 and 11/02/2012. Panel C is between 09/02/2017 and 11/02/2017. Panel D is between 09/02/2020 and 11/02/2020. The innermost black line shows the average magnetopause prediction using the Roelof and Sibeck (1993) model, the outermost shows the boundary to the magnetosheath. The numbers on the orbit show the day of the year for that point of the orbit. Taken from SSC Web (Satellite Situation Center Web, NASA)

- Active Spacecraft POtential Control experiment, ASPOC
  Charged particle emitters that cancel out the electric charge the satellites accumulate, due to exposure to solar wind and plasma within the magnetosphere

- Cluster Ion Spectrometry experiment, CIS
  Analysed the composition, mass and distribution of particles encountered by the spacecraft. Consisted of a Hot Ion Analyser (HIA) and a COmposition and DIstribution Function analyser (CODIF). This instrument failed on Cluster 2

- Electron Drift Instrument, EDI
  Fired two beams of electrons into space, which after an orbit of 10km returned to the spacecraft, allowing the measurement of the strength of the electric and magnetic fields around each of the four spacecraft

- Plasma Electron And Current Experiment, PEACE
  Similar to CIS focusing on low to medium energy electrons, measuring their trajectory and counting them

- Research with Adaptive Particle Imaging Detectors, RAPID
  Particle detector measuring the highest energy electrons and charged particles. They pass through pinholes to reach the detector: gives information of where the particles came from

- Wave Experiment Consortium, WEC (Instruments I, ESA)
  Five of the instruments designed for measuring electric and magnetic fields and waves, grouped under the WEC name:

  - Digital Wave Processing experiment, DWP
    The control of the WEC, providing precise timing and computing. Includes a particle correlator allowing variations in the electron population around the spacecraft to be compared with measured waves
  - Electric Field and Wave experiment, EFW
    Uses electric sensors on 42 m wire booms to measure electric fields and waves, revealing the density of nearby electrons
  - Spatio-Temporal Analysis of Field Fluctuation experiment, STAFF
    Magnetometer that can measure variations in the magnetic field. These occur in regions where the solar wind and magnetosphere interact
  - Wide Band Data instrument, WBD
    Provides high resolution measurements of electric and magnetic fields at certain frequency bands. Listens to radio whistles and hisses of particles that bounce near Earth's magnetic poles

– Waves of HIgh frequency and Sounder for Probing of Electron density by Relaxation experiment, WHISPER
Uses radar to measure the density of charged particles. Radio pulses are sent through the wire booms, triggering oscillations that are measured after a delay

All of these instruments are fitted to each of the four Cluster spacecraft in the same arrangement, allowing for comparison of measurements between each satellite, giving a view of the area covered between the spacecraft.

2.2.2 Cluster's Orbit

The four Cluster spacecraft occupy highly elliptical polar orbits, each with an apogee (at the time of launch) of 19.7 Re and perigee of 4.0 Re. The plane of each spacecraft's orbit is fixed in inertial space such that the major axis drifts through 24 hours of local time every 12 months, allowing the satellites to visit a range of magnetospheric regions each year. Over the 14 years of science operations, orbital evolution and planned manoeuvres reduced the typical perigee and apogee to 3.5 Re and 17.4 Re, respectively (e.g. Cluster II, NASA; Cluster II operations, ESA). This then continued to evolve as the science operations continued until 2024 when the first satellite (Salsa) manoeuvred into its final orbit (e.g. Goodnight Cluster: brilliant end to trailblazing mission, ESA).

The red line in figure 2.3 represents two of Cluster's orbits between 31/05/2012 and 05/06/2012, with the numbers showing the day of the year. Each panel in figure 2.3 shows a different plane, which combined represents the orbit in all three dimensions of GSE coordinates: Panel A is the X-Y plane looking at the equatorial plane viewed from above North. Panel B is the X-Z plane looking at the noon-midnight meridian viewed from dusk. Panel C is the Y-Z plane looking at the dawn-dusk plane, viewed from the Sun. Panel D is the X-ρ plane where the ρ parameter is defined by equation 2.1.

$$\rho = \sqrt{Y_{GSE}^2 + Z_{GSE}^2} = \sqrt{Y_{GSM}^2 + Z_{GSM}^2} \tag{2.1}$$

Since the spacecraft are locked to inertial space the orbit changes in relation to Earth, as the year progresses with the orbit rotating around the X-Y plane. Figure 2.4 shows the X-Y plane of Cluster's orbit, at four different points during the year. Panel A is between 31/05/2012 and 05/06/2012 as seen in figure 2.3. Panel B is between 31/08/2012 and 05/09/2012. Panel C is between 30/11/2012 and 05/12/2012. Panel D is between 28/02/2013 and 05/03/2013. It can be seen that the orbit rotates around Earth during the year, from the dawn flank, to the nightside, to the dusk flank, then to the dayside in this case.

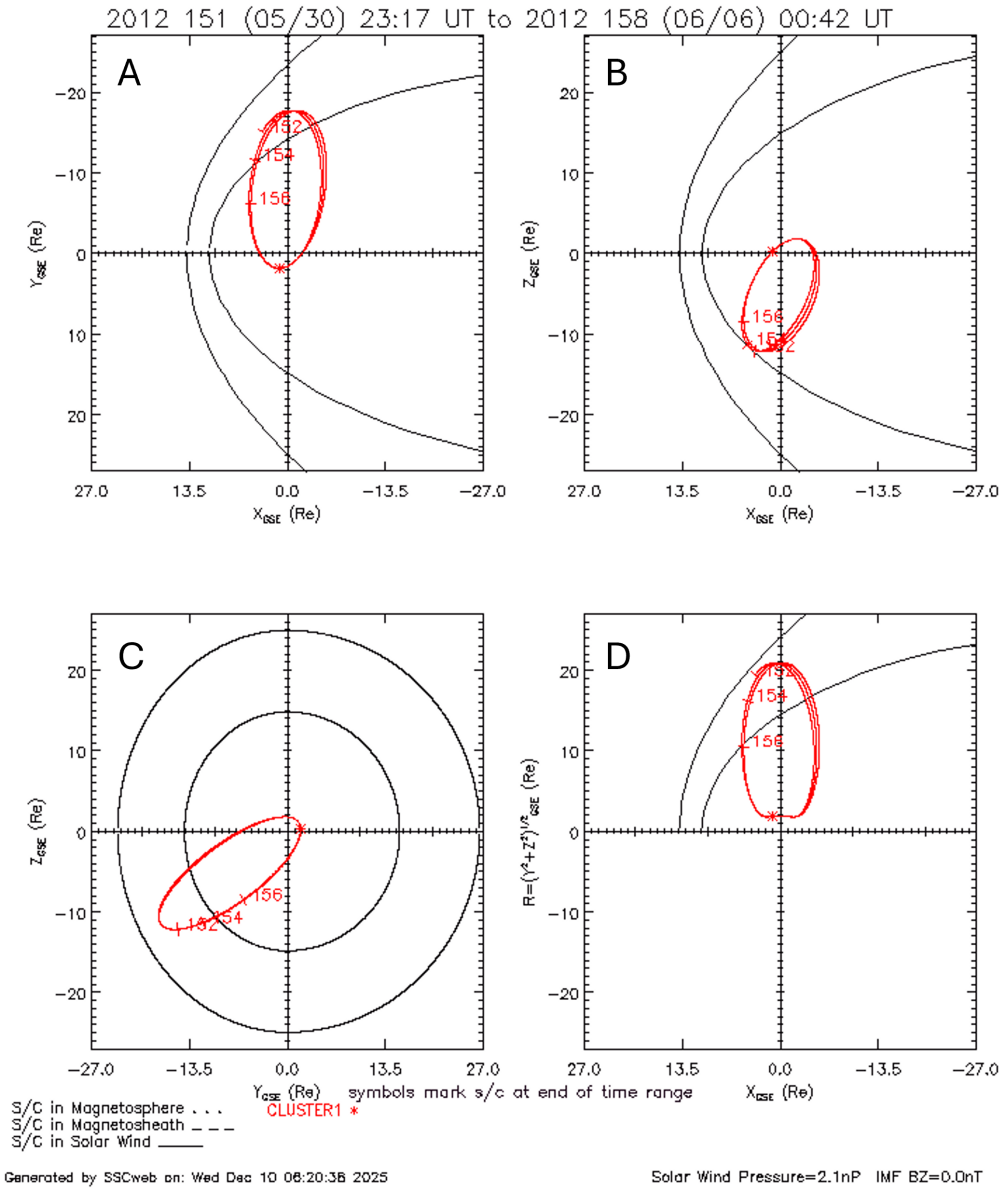

Figure 2.3: View of a typical Cluster 1 orbit, shown in red, starting on 31/05/2012. This is shown in the X-Y plane in panel A, X-Z in panel B, Y-Z in panel C, and X-ρ in panel D. The ρ parameter is described by equation 2.1, where ρ is calculated from the Y and Z components. Shown in GSE coordinates. The innermost black line shows the average magnetopause prediction using the Roelof and Sibeck (1993) model, the outermost shows the boundary to the magnetosheath. The numbers on the orbit show the day of the year for that point of the orbit. Taken from SSC Web (Satellite Situation Center Web, NASA)

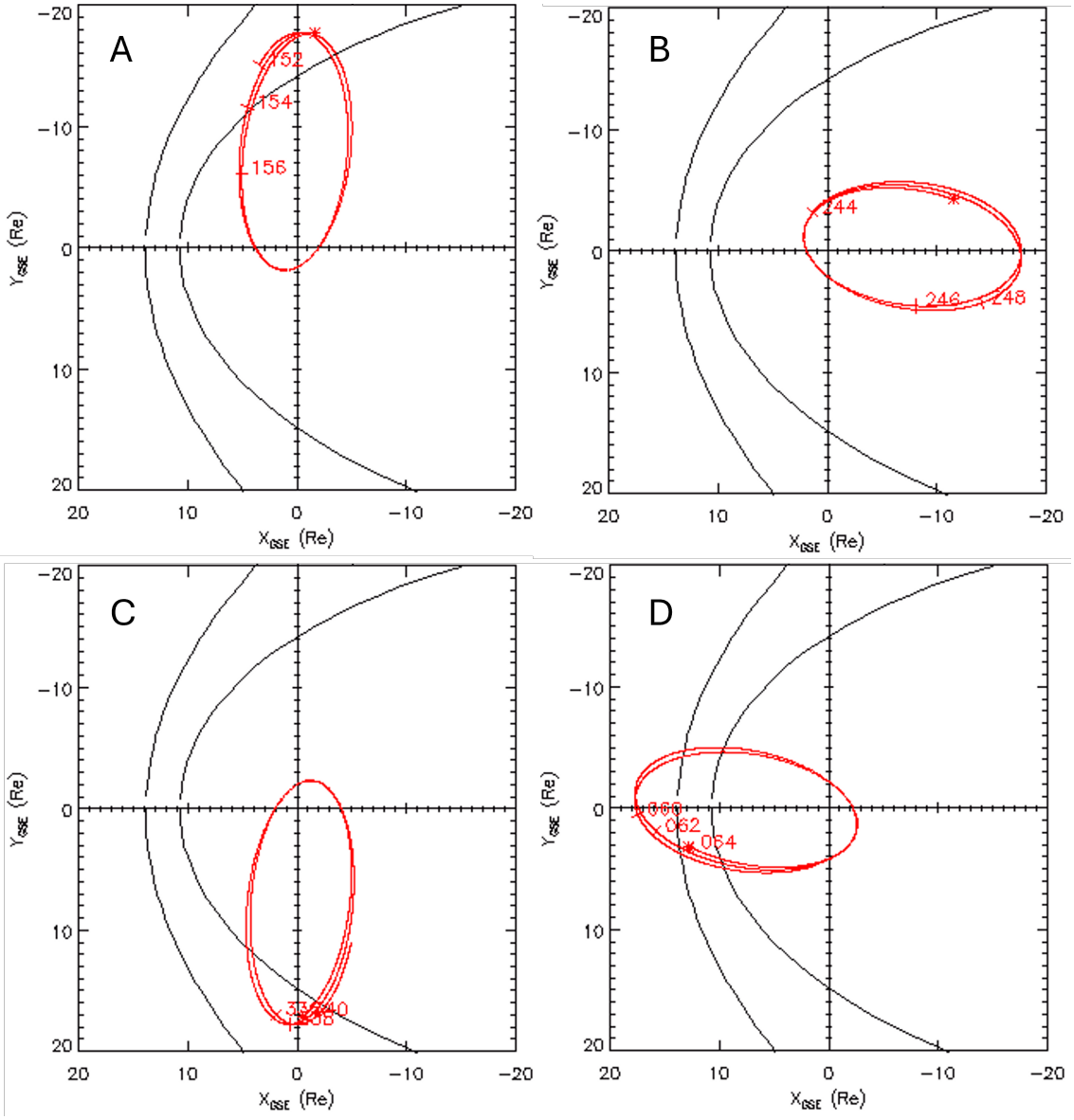

Figure 2.4: The evolution of the orbit through the year, shown with the orbit at four different times, in the X-Y GSE plane. Panel A is between 31/05/2012 and 05/06/2012 as seen in figure 2.3. Panel B is between 31/08/2012 and 05/09/2012. Panel C is between 30/11/2012 and 05/12/2012. Panel D is between 28/02/2013 and 05/03/2013. The innermost boundary is a prediction of the magnetopause position using the Roelof and Sibeck (1993) model, the outermost boundary is the start of the magnetosheath. The numbers show the day of the year the orbit is at. Taken from SSC Web (Satellite Situation Center Web, NASA)

In GSM coordinates, some oddities emerge when you analyse the orbit of a spacecraft. Figure 2.5 shows a typical Cluster orbit shape in the GSM coordinate system. For the X-Y and X-Z planes, the path follows a typical elliptical orbit that you would expect in GSE coordinates, except for a indentation towards the centre of orbit. Both occur near X=0, with positive Y for the X-Y plane and negative Z for the X-Z plane. The Y-Z plane path doesn't look like a typical GSE orbit, however, with many irregular changes of direction. The X-ρ plane is identical to what it would be in GSE coordinates, as any change made to the Y axis when converting to GSM coordinates is cancelled out by the change done to the Z axis, for the calculation of ρ. Additionally, the X axis is invariable when comparing between GSE and GSM coordinates.

2.3 OMNI Solar Wind

The solar wind data used in this investigation originates from the OMNI solar wind dataset. This dataset comes from a wide range of satellites including: ACE, IMP 8, WIND and Geotail (e.g. King and Papitashvili). These satellites orbit Lagrange point 1 between the Earth and Sun: a point of equilibrium for the gravitational forces between the Earth and Sun (e.g. Cornish, 1998). This is done to provide an optimum point to measure the solar wind on the path towards Earth. These spacecraft provide measurements of both magnetic field (X, Y and Z magnetic field strength components) and plasma (including flow pressure, temperature, *etc.*) of the solar wind, which are then time shifted to predict the conditions at Earth's bow shock. This time shift is calculated through equation 2.2.

$$\Delta t = \mathbf{n} \cdot \frac{(\mathbf{P}_T - \mathbf{P}_O)}{\mathbf{n} \cdot \mathbf{V}_{SW}} \tag{2.2}$$

In equation 2.2, Δt is the time shift, $\mathbf{n}$ is the eigenvector normal to the solar wind wave front, $\mathbf{P}_T$ is the target position, $\mathbf{P}_O$ is the position of the OMNI spacecraft and $\mathbf{V}_{SW}$ is the solar wind velocity. This equation will allow the measured time of each point of data to be translated to the predicted time the solar wind will reach Earth. This is done for each of the spacecraft individually for each data point they have gathered, as they will be in different positions around Lagrange point 1.

2.4 Geospace Region and Magnetospheric Boundary Identification Dataset

In order to analyse the Cluster data the work done by Grison *et al.* (2025) has been used. In their 2025 paper, they found the location of Cluster within Earth's magnetic environment,

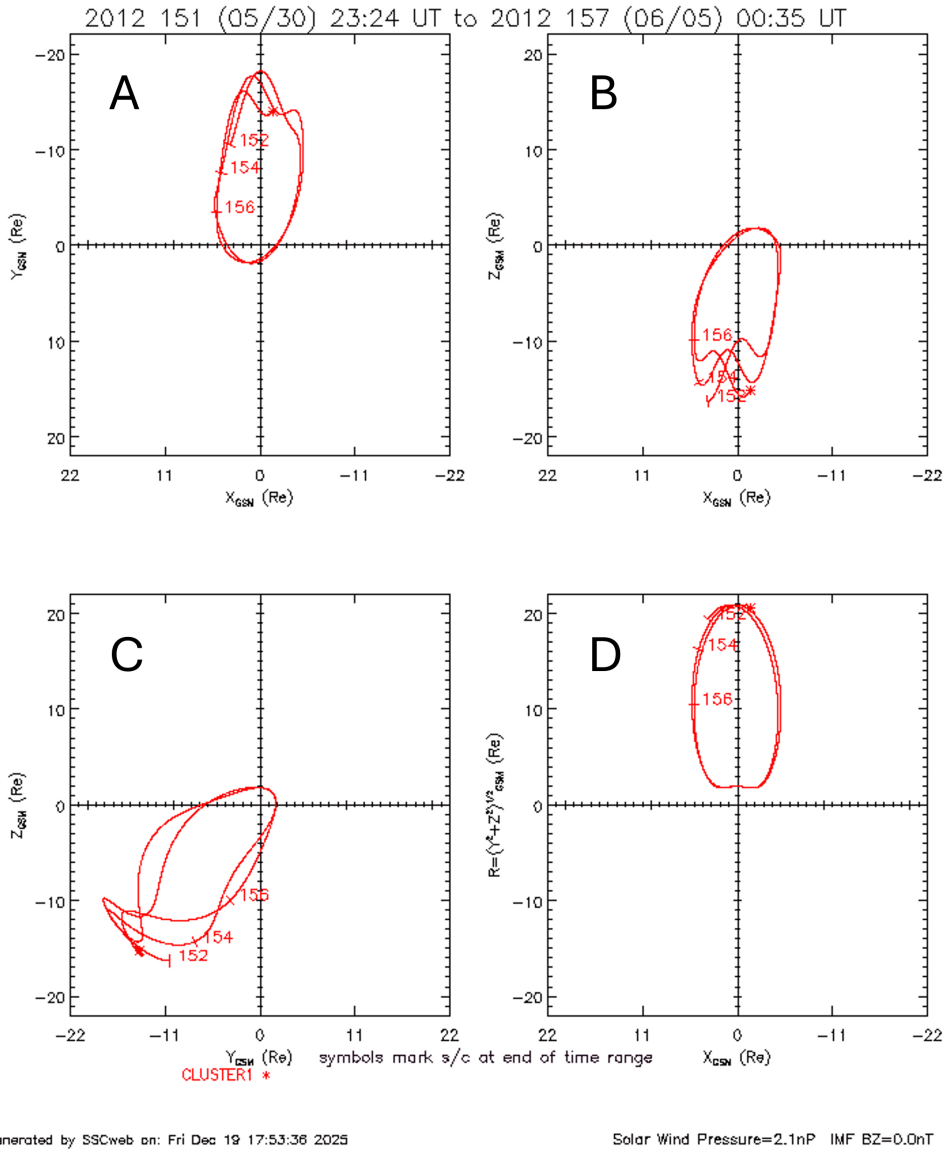

Figure 2.5: View of a typical Cluster 1 orbit, shown in red, in GSM coordinates; starting on 31/05/2012. Panel A shows the X-Y plane. Panel B shows the X-Z plane. Panel C shows the Y-Z plane. Panel D shows the X-ρ plane. This has been done to demonstrate that orbits in GSM coordinates are not the typical elliptical shape as shown in GSE coordinates, which can be seen in panels A, B and C. Panel D is identical to what would be seen in GSE coordinates, as any change made to the Y axis when converting to GSM coordinates is cancelled out by the change done to the Z axis, for the calculation of ρ (found in equation 2.1). Taken from SSC Web (Satellite Situation Center Web, NASA)

for each point in Cluster's mission. This was done by manually looking at the data from the magnetometers to find changes in the magnetic field strength associated with transitioning between regions.

Looking at the magnetic field strength in figure 2.6, the transition can be understood. There is a highly variable magnetic field strength outside the magnetosphere and a relatively consistent one inside the magnetosphere. This transition is shown with the B_x and $|B|$ components in figure 2.6, as the graph shows a transition from within the magnetosphere to outside the magnetosphere, when the magnetopause transition region (MPtr) line is crossed. Within the density and energy of protons the transition can also be seen, as they go from low to high densities and energies, when transitioning from inside the magnetosphere to outside. Using these identifying parameters, each start of a magnetopause crossing can be found which, when paired with the next region transition (either the magnetosheath or a region inside the magnetosphere), can create a list of times representing each magnetopause crossing.

From this they created the Geospace Region and Magnetospheric Boundary identification (GRMB) dataset, of Cluster's location during the mission. The locations are denoted by "location tags": such as IN/PLS (Plasmasphere), or OUT/MSH (Magnetosheath); with IN and OUT representing whether Cluster is inside or outside the magnetosphere (Grison *et al.*, 2025). Several of these regions had related "transition regions", such as the IN/MPtr for the magnetopause transition region, with their own location tag in dataset. These are regions in which the conditions associated with two different environments are found in the same area; for the magnetopause transition region there will be conditions relating to the plasmasheet and magnetosheath found. This causes the identification of the region to be complex and potentially causing confusion with other regions. This complexity is enhanced by the angle at which Cluster approaches the magnetopause: at some points Cluster skims the edge of the magnetopause, which, due to variation in magnetopause location, causes repeated crossings. This would create many recorded transitions when only one is necessary. The GRMB dataset accounts for this skimming behaviour by labelling the entire period of skimming as within the magnetopause transition region; this could be the cause of some longer transitions investigated further in section 3.3.2 and seen in figure 3.3.

Therefore, for this investigation, the magnetopause and magnetopause transition region location tags were used to determine when Cluster crossed the magnetopause. Using the magnetopause transition region introduces uncertainties, due to the large zone in which the magnetopause can be found, when compared to the thickness of the magnetopause. However, this is necessary to produce a large enough dataset to be certain of the results; and the larger uncertainties emerging from this have been accounted for during the investigation, discussed in section 3.3.2.

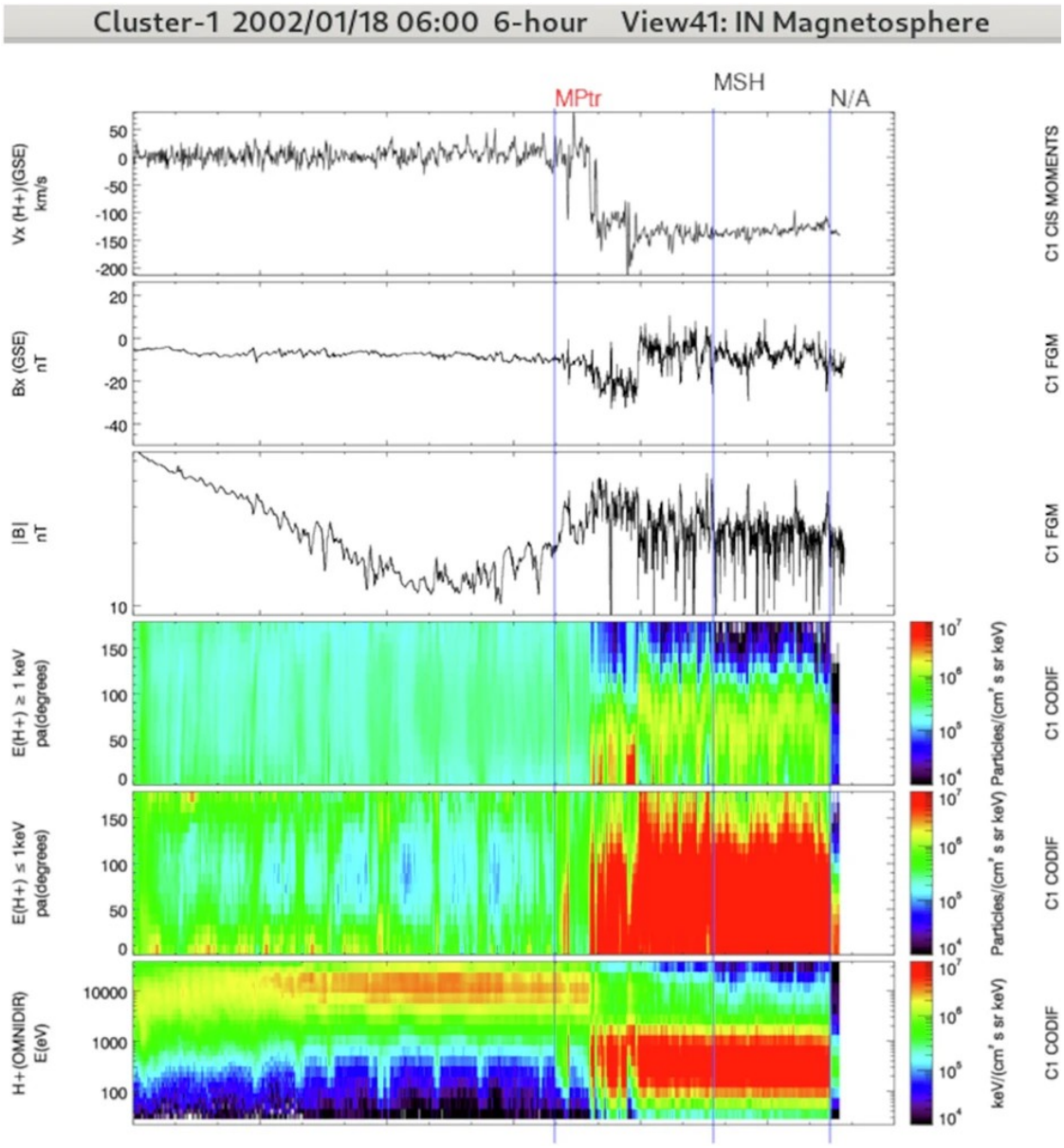

Figure 2.6: Taken from Grison *et al.* (2025). A section of the magnetic data from Cluster 1 showing a crossing of the magnetopause. The X component of the magnetic field strength and the overall magnetic field strength can be seen, as well as the energy, densities and X component of the velocity of protons in the surrounding environment. Crossing the magnetopause trasition region from outside the magnetosphere to inside the magnetosphere, there is a change from calmer conditions to more variable conditions across all of the parameters observed

The crossings found in the GRMB dataset can then be compared with the positional data from the Cluster archive. This position data has a resolution of 1 minute, is expressed through GSE coordinates, and includes the time associated with those positions. Through this process, the locations of where Cluster crosses the magnetopause can be determined and analysed. Firstly, this is done by finding what orbital position the Cluster spacecraft are in when they encounter the magnetopause. This can be seen in Figure 2.7.

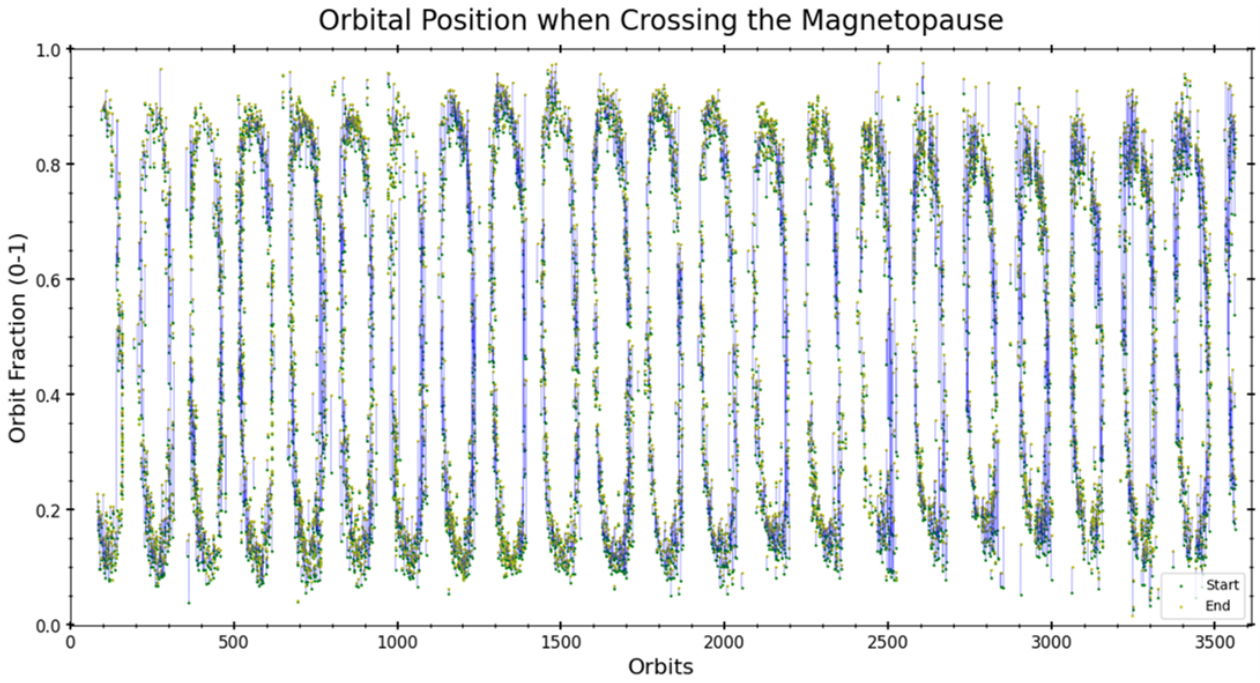

Figure 2.7: Magnetopause crossings as Cluster's orbit evolves during the entire mission. The orbital fraction is how far through its orbit Cluster has travelled, with 0 as the apogee and 0.5 as the perigee. The green points are the start of a magnetopause crossing, the yellow points are the end with the blue line connecting the two. A repeating pattern can be seen, showing how the crossings evolve through the year: explored further in the text

Figure 2.7 was created by finding the orbit numbers of each transition, including the fraction of the orbit number: showing which orbit Cluster is on and how far through the orbit Cluster is. The integer value of each orbit number can be taken away to leave the fraction of the orbit, showing only how far through the orbit Cluster is found. This is then plotted on the Y axis, the original orbit value plotted on the X axis, to give the Bryant plot shown. Therefore, figure 2.7 is an expression of how the magnetopause crossings change in comparison to Cluster's orbit.

In figure 2.7, there is a repeating pattern that emerges, where the crossings occur primarily half way through Cluster's orbit, shifting to the start or end of Cluster's orbit. The crossings then return to occurring half way through Cluster's orbit, before there are no encounters with the magnetopause. This pattern can be seen clearly taking a two year segment of the mission, as seen in figure 2.8.

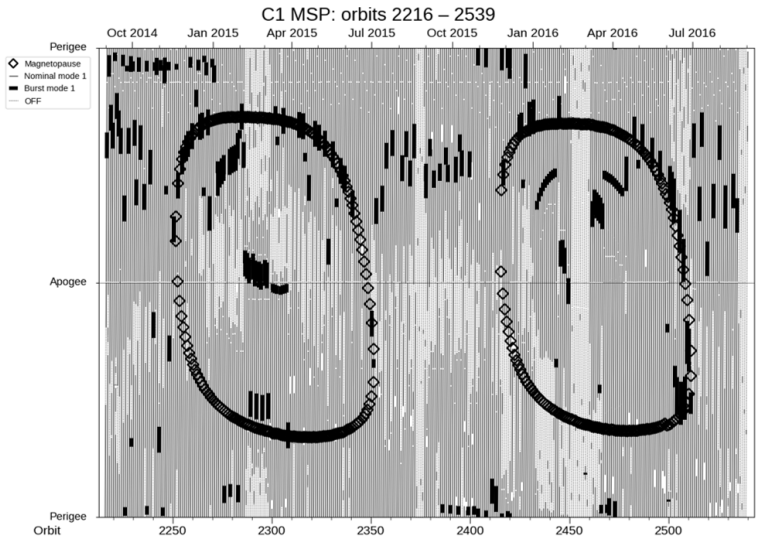

Figure 2.8: Magnetopause crossings as Cluster's orbit evolves between September 2014 and September 2016. The Y axis shows how far through the orbit Cluster 1 has travelled. The X axis is the number of orbits covered, including the fraction of the orbit. The magnetopause crossings are shown with a diamond shaped point. The lines from top to bottom represent what mode Cluster 1 is in at that period of time, differentiated by the thickness of the line

Given the shape of the magnetopause and Cluster's orbit, the absence of any magnetopause crossings suggests Cluster is orbiting within the magnetotail. Then as Cluster's orbit starts to shift around Earth, the orbit starts to encounter the magnetopause at apogee, half way through the orbit. There will also be some crossings somewhat closer to the start or end of the orbit in cases such as the X-Y graph in figure 2.3. At the flanks (sides) of the magnetopause and the mid latitudes, the magnetopause will be encountered somewhere between apogee and perigee and will cause the crossings at around 0.25 and 0.75 in orbital fraction, found in figure 2.7. By the time Cluster's orbit is near the nose of the magnetosphere, the magnetopause will only be encountered towards the start and end of the orbit. The crossings will occur closer to perigee and the apogee will be much larger than the magnetopause standoff distance (distance to the nose of the magnetopause).

2.5 Magnetospuse Models

2.5.1 The Shue Model

The first of the models that will be compared to Cluster is the Shue *et al.* (1998) model (adapted from the Shue *et al.* (1997) model). This model is a cylidrically symmetric, empirically derived magnetopause surface based on data from 8 satellites including ISEE 1, 2 and 3, AMPTE/IRM, GOES 2, 5 and 6 and IMP 8. From this data, equations were found for the standoff distance (r_0) and the tail flaring angle (α, how much the magnetotail extends outwards from a centre line, where $\alpha = 0.5$ would result in a constant magnetosphere size). This uses the Z component of the magnetic field strength (B_z) and dynamic pressure (D_p) of the solar wind, shown in equation 2.3 and equation 2.4.

$$\alpha = (0.58 - 0.007B_z)(1 + 0.024\ln[D_p]) \tag{2.3}$$

$$r_0 = [10.22 + 1.29\tanh(0.184(B_z + 8.14))](D_P)^{-\frac{1}{6.6}} \tag{2.4}$$

These calculations are for singular instances of the solar wind conditions, which will pair with one Cluster data point. The standoff distance and tail flaring angle can then be combined to find the distance of the predicted magnetopause from the centre of Earth ($\mathbf{r}$), at a specific angle (θ) defined as the angle between the Earth-Sun line and the distance $\mathbf{r}$. An entire magnetopause can be predicted by using a range of θ values with specific r_0 and α values. This is calculated by using equation 2.5.

$$\mathbf{r} = r_0 \left(\frac{2}{(1 + \cos\theta)} \right)^{\alpha} \tag{2.5}$$

These equations aren't dependant on the differences between GSE and GSM coordinates as the $\mathbf{r}$ and θ parameters are defined in the X-ρ plane. Solar wind aberration (shift in the magnetosphere position within the ecliptic plane based on Earth's orbital motion around the Sun) is accounted for in the Shue model via equation 2.6, where V_{es} is the velocity of Earth around the Sun ($30 kms^{-1}$), and V_{sw} is the solar wind velocity.

$$\theta_{aberr} = \tan^{-1}\left(\frac{V_{es}}{V_{sw}}\right) \tag{2.6}$$

Using equations 2.3, 2.4, 2.5 and the solar wind data from the OMNI dataset, many predicted magnetopause surfaces can be found using various dynamic pressures and IMF B_z.

2.5.2 Asymmetrical Models

Two other models are used during this investigation which are asymmetrical models, allowing the analysis of the magnetospheric cusp region. These include the Lin *et al.* (2010) model and the Liu *et al.* (2015) model. The inclusion of the cusp region results in more complex models than the Shue model, as more variables are involved with a larger number of equations, but are still models that can be easily computed.

Earth's dipole tilt angle (angle at which the magnetic field dipole is found compared to the GSM Z axis (e.g. Eggington *et al.*, 2020)) is the common variable between the Lin and Liu models that isn't included in the Shue model. The inclusion of this variable will allow for differences between the northern and southern hemispheres, as it will account for the angle the magnetosphere is tilted at. For both models, a radius (r) value is found at angles θ and ϕ, which have been defined differently dependant on the model.

2.5.2.1 The Lin Model

For the Lin *et al.* (2010) model, the coordinates are defined where "r is the radial distance at a zenith angle (θ) between the direction of r and the positive X direction" and the "azimuth angle (ϕ)", as seen in figure 2.9.

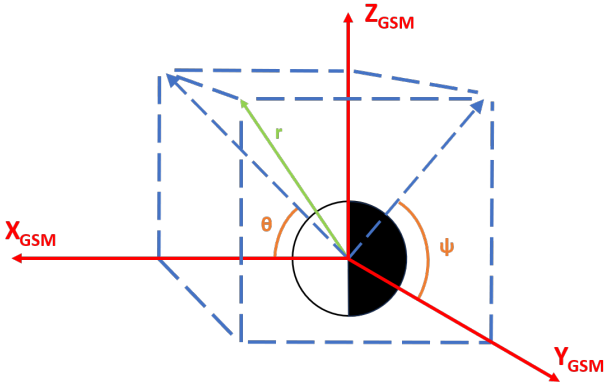

Figure 2.9: Diagram showing how the distance (r) to the magnetopause is calculated in the Lin model. This is defined in corrected GSM coordinates accounting for the solar wind aberration

This model includes data from a wider range of sources than the Shue model. This includes Cluster, Geotail, GOES, IMP 8, Interball, LANL, Polar, TC1, THEMIS, and Wind; while using solar wind data from ACE and Wind. The data collected is used within a transformed version of GSM coordinates, accounting for the solar wind aberration.

They have used the magnetic and dynamic pressures, IMF B_z and dipole tilt angle to determine r. The magnetic pressure seemed to have a negligible difference in the size of the magnetopause for the purposes of this investigation. Therefore, the differences found will likely arise from the inclusion of the dipole tilt angle and the complexity of the model, compared to the Shue model.

2.5.2.2 The Liu Model

The Liu *et al.* (2015) model uses the Space Weather Modelling Framework (SWMF) magnetohydrodynamic code to simulate the magnetosphere system and determine the location of the magnetopause, within the GSM coordinate system. They use all magnetic field strength components of the solar wind (B_x, B_y and B_z), the dynamic pressure and the dipole tilt angle. This may allow for a higher complexity, with the inclusion of more variables than both the Shue model and the Lin model.

The Liu model, defines the coordinates as "r is the radial distance from the centre of the Earth, the polar angle θ measures the angle with respect to the Earth-Sun line, and the azimuth angle ϕ measures the angle from the positive Z axis", as seen in figure 2.10.

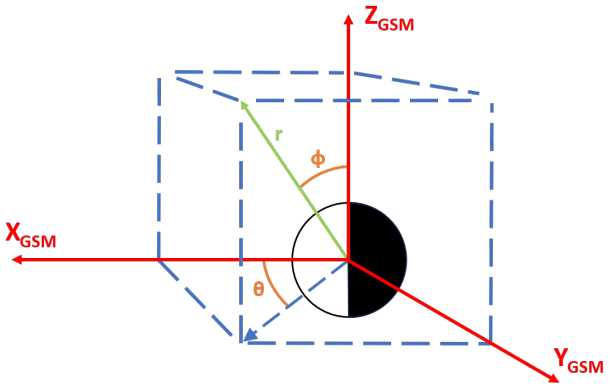

Figure 2.10: Diagram showing how the distance (r) to the magnetopause is calculated in the Lin model. This is defined in GSM coordinates

2.5.3 Model Shapes

Figure 2.11 shows all three magnetopause models in the X-Y, X-Z and Y-Z planes. This is under fixed solar wind conditions of: B_x = 10nT, B_y = 1nT, B_z = -5nT, D_P = 2nPa and a fixed dipole tilt angle of 0^o. Within the X-Y plane, figure 2.11 shows that the Liu model

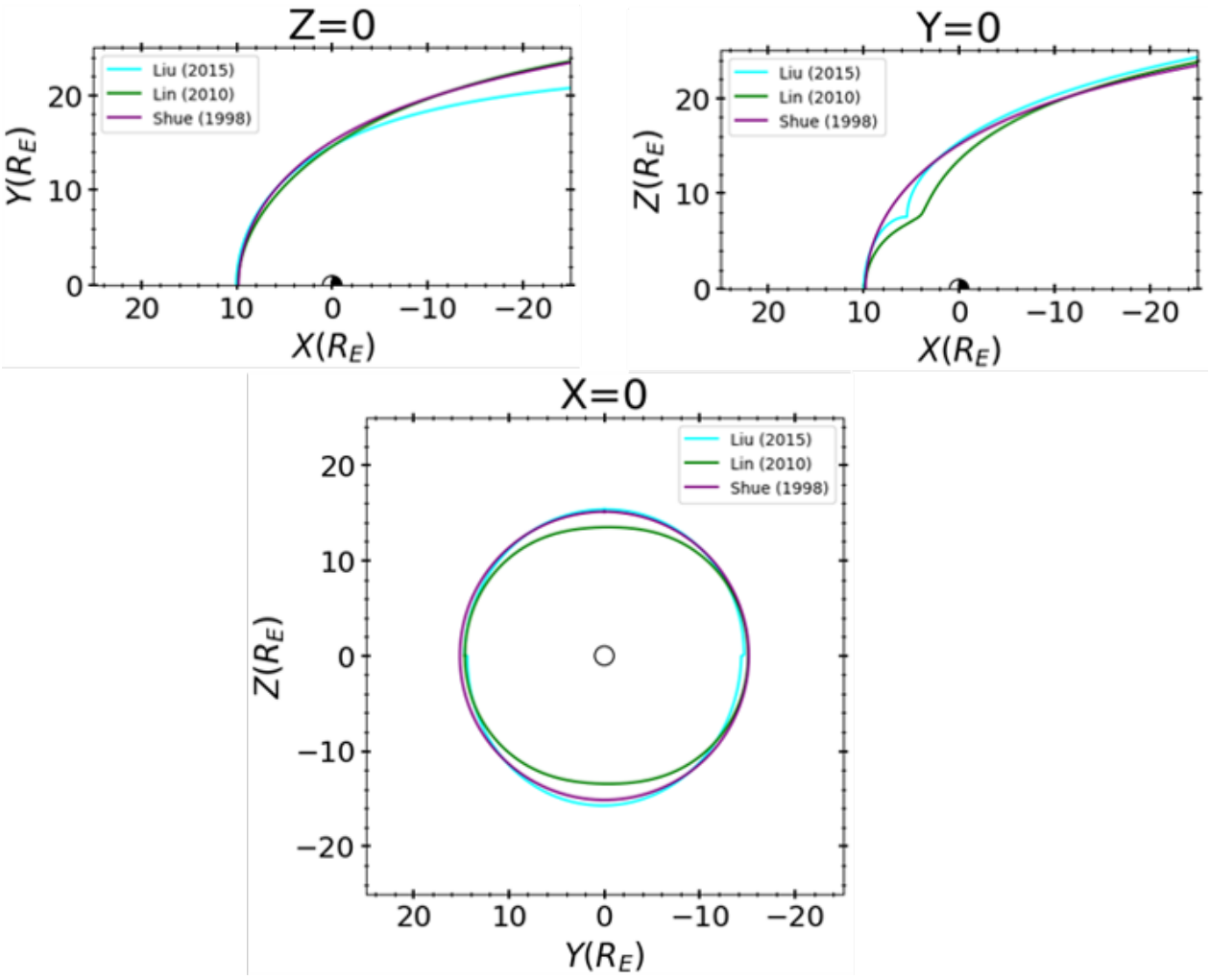

Figure 2.11: All three magnetopause models in the X-Y, X-Z and Y-Z planes, with fixed solar wind conditions: B_x = 10nT, B_y = 1nT, B_z = -5nT, D_P = 2nPa and a fixed dipole tilt angle of 0^o

has a slightly larger standoff distance, but less tail flaring compared to the Lin model, under similar solar wind conditions. This is determined since the magnetopause is slightly larger at the nose, but much smaller by the magnetotail. In the X-Z plane there is a similar difference with the standoff distance. Furthermore, a sharper angled and more pronounced cusp region is observed in the Liu model, shown by the large dip towards Earth in the magnetopause. Eventually, the size difference between these models returns to similar levels prior to the cusp region. For the Y-Z plane the Lin model is much smaller along the Z axis, but slightly larger along the Y axis. The Liu model is much more circular in this plane, suggesting it has a blunter nose than the Lin model. There is a distinct difference between the northern

and southern hemisphere for the Liu model with the northern hemisphere magnetopause expanding further than the southern. The Shue model follows a similar trend to the Lin model in the X-Y plane, and the Liu model in the Y-Z plane. For the X-Z plane, the Shue model initially follows the trend of the Liu model; this then diverts with the inclusion of the cusp region in the Liu and Lin models, with Shue producing a smooth curve. Towards the tail in this plane the Shue model follows the trend shown by the Lin model.

Chapter 3

Results

3.1 Cluster Position During a Crossing

Using the understanding of Cluster's orbit and the crossings of the magnetopause, the shape of the magnetopause according to Cluster can be found. To achieve this, the GRMB dataset can be compared with the position data from ESA. This is done by finding the closest matching time within the Cluster archive to each point in the GRMB dataset, then using the position associated with this time to find where Cluster is when crossing the magnetopause. The X, Y and Z coordinates are then found for each crossing of the magnetopause in GSE coordinates.

A limit is placed on the data based on the length of each magnetopause crossing. This is to exclude any anomalous crossings that appear to be too long for a magnetopause crossing; investigated further in section 3.3.2. Figure 3.1 is produced to determine an initial length to use and shows that 50% of crossings are less than 49 minutes. Therefore, any magnetopause crossing shorter than 49 minutes is temporarily used in the analysis. This method can also be used to determine other proportions of the data used in the analysis, determined later when the best compromise between the uncertainty and number of data points is found, in section 3.3.2.

Using the method outlined at the start of this section and the limit imposed on the data, figure 3.2 shows the distribution of magnetopause locations. Here, there are four different views of the magnetopause. This uses the same layout shown in figure 2.3 as described in section 2.2.2. Panel D gives a representational view of the magnetopause in all 3 dimensions while using only two dimensions, as it combines the Y and Z axes. This is a useful method to more simply analyse the structure of the magnetopause unchanging between GSE and GSM coordinates; therefore, the ρ parameter will be useful as the analysis progresses.

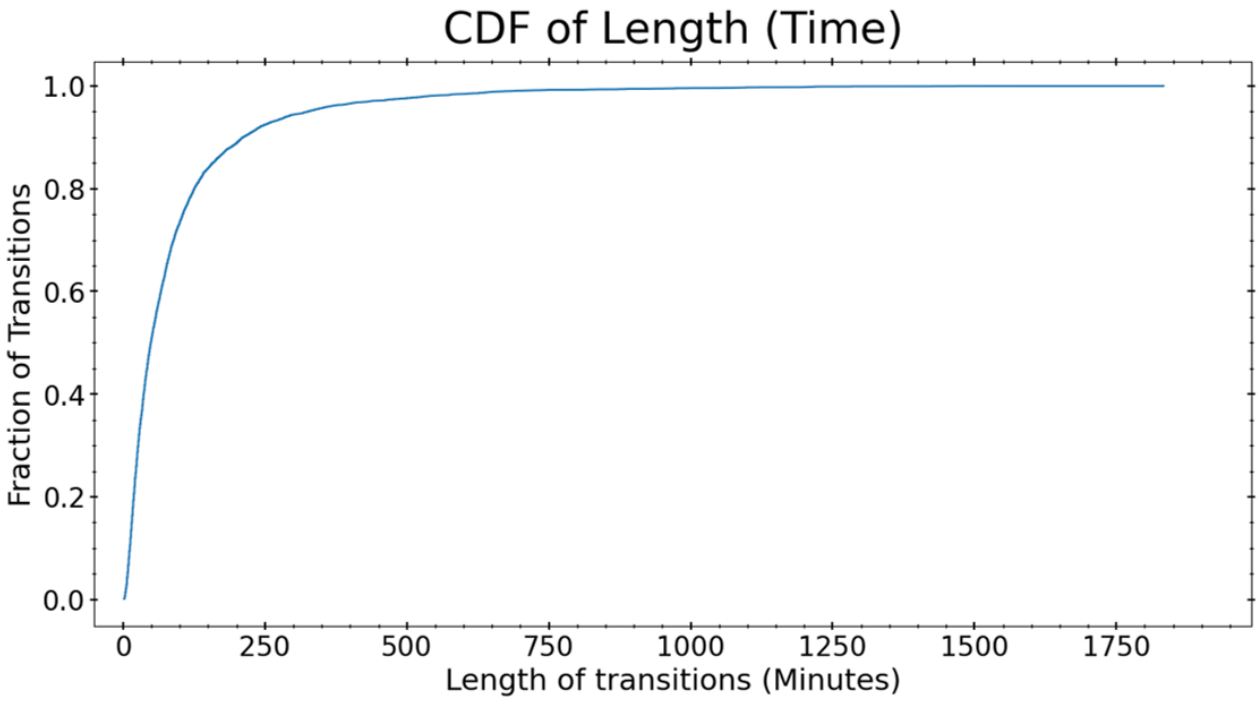

Figure 3.1: Cumulative distribution function for the transition duration of magnetopause crossing events. 50% of events have a magnetopause crossing transition duration of 49 minutes or less. A very small proportion of events have magnetopause crossing transitions that span more than 2 hours, with some transitions occurring for more than a Cluster orbital period

For figure 3.2 the data has been limited to 50%. Each crossing has a varied length: depending on Cluster's trajectory compared with the shape of the magnetopause. Therefore, Cluster can be within the magnetopause transition region for a varying amount of time, causing uncertainty where the magnetopause might be. This is investigated within section 3.3.2, where the optimal percentage of the data to use is determined, balancing the uncertainty and amount of data.

3.2 GRMB Dataset Analysis

With the GRMB dataset as a new addition to the Cluster archive, the validity and precision of this dataset needs to be determined. The fact that some of the crossings span a large time frame, shown in figure 3.1, proves that some of the results may not be reliable, due to high uncertainty. This proves the dataset needs investigating.

Given that this dataset has been manually created, via analysis of the magnetic data, there

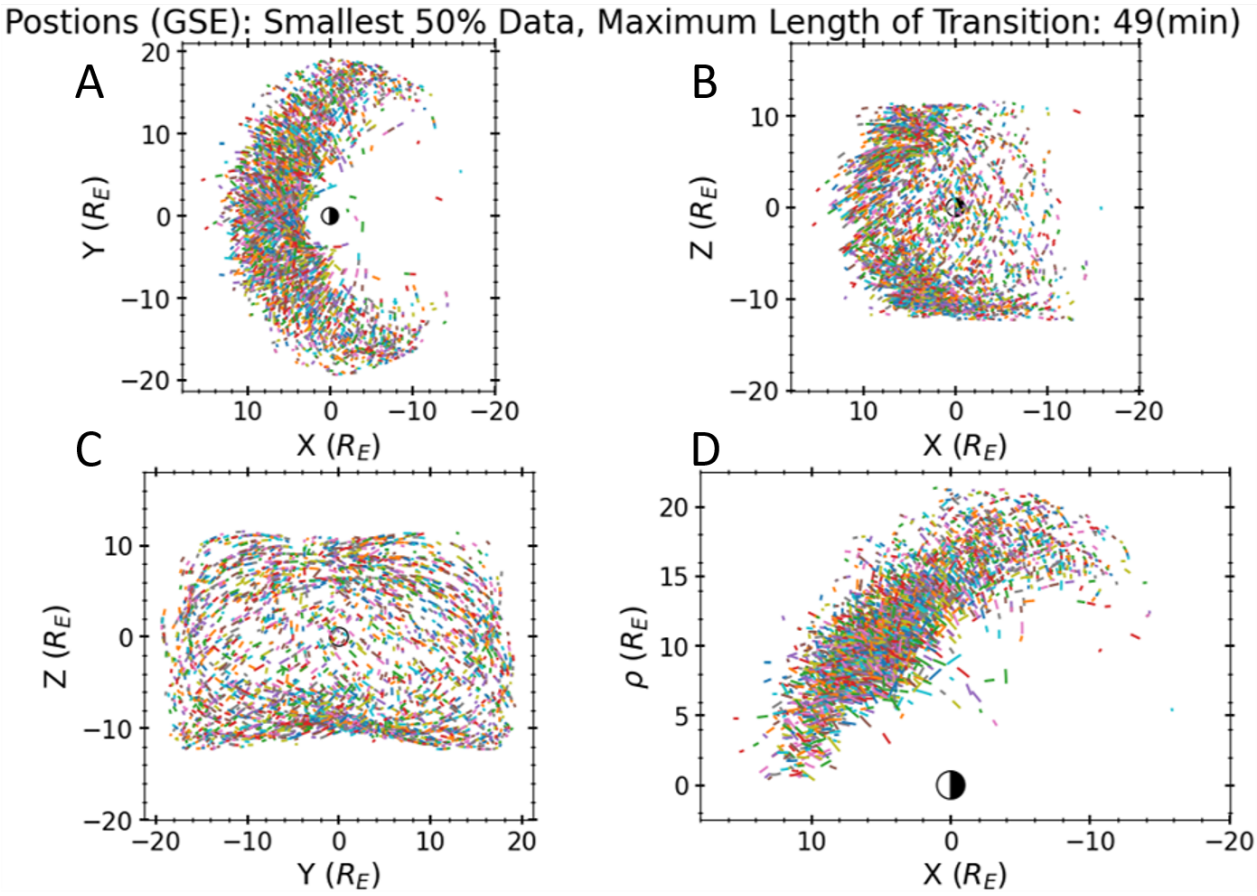

Figure 3.2: Magnetopause crossings represented in four different planes within GSE coordinates. Panel A is the X-Y plane, panel B is the X-Z plane, panel C is the Y-Z plane, and panel D is the X-ρ plane; where ρ is described by equation 2.1. This is for the shortest 50% of magnetopause crossings based on time Cluster is within the magnetopause region. There is no meaning behind the different colours for each crossing, other than ease of identification of individual crossings

will be a number of advantages and drawbacks compared to algorithmically derived datasets. An algorithm will produce a dataset much faster, however, the algorithm may include more errors, due to the complexity of creating an algorithm identifying a magnetopause crossing, and may not compute crossings where a parameter is missing. However, there is the possibility of data entry error with the method used in creating the GRMB dataset. Both data entry and algorithm based errors could occur with misidentifying a transition between regions when there is none, or missing when a transition occurs. If a transition is missed, the region will be much longer than expected, potentially leading to the longer crossings found within figure 3.1. Alternatively, a misidentified transition could lead to regions mislabelled as other

regions. This would lead to magnetopause crossings wrongly located and with the wrong proportions, changing the averages. With consideration of the potential inaccurate crossings, the manual method of dataset creation can allow the avoidance of many disadvantages with algorithmically produced datasets. However, inaccurate crossings within the GRMB dataset have to be accounted for to avoid incorrect conclusions.

3.2.1 GSM Orbit

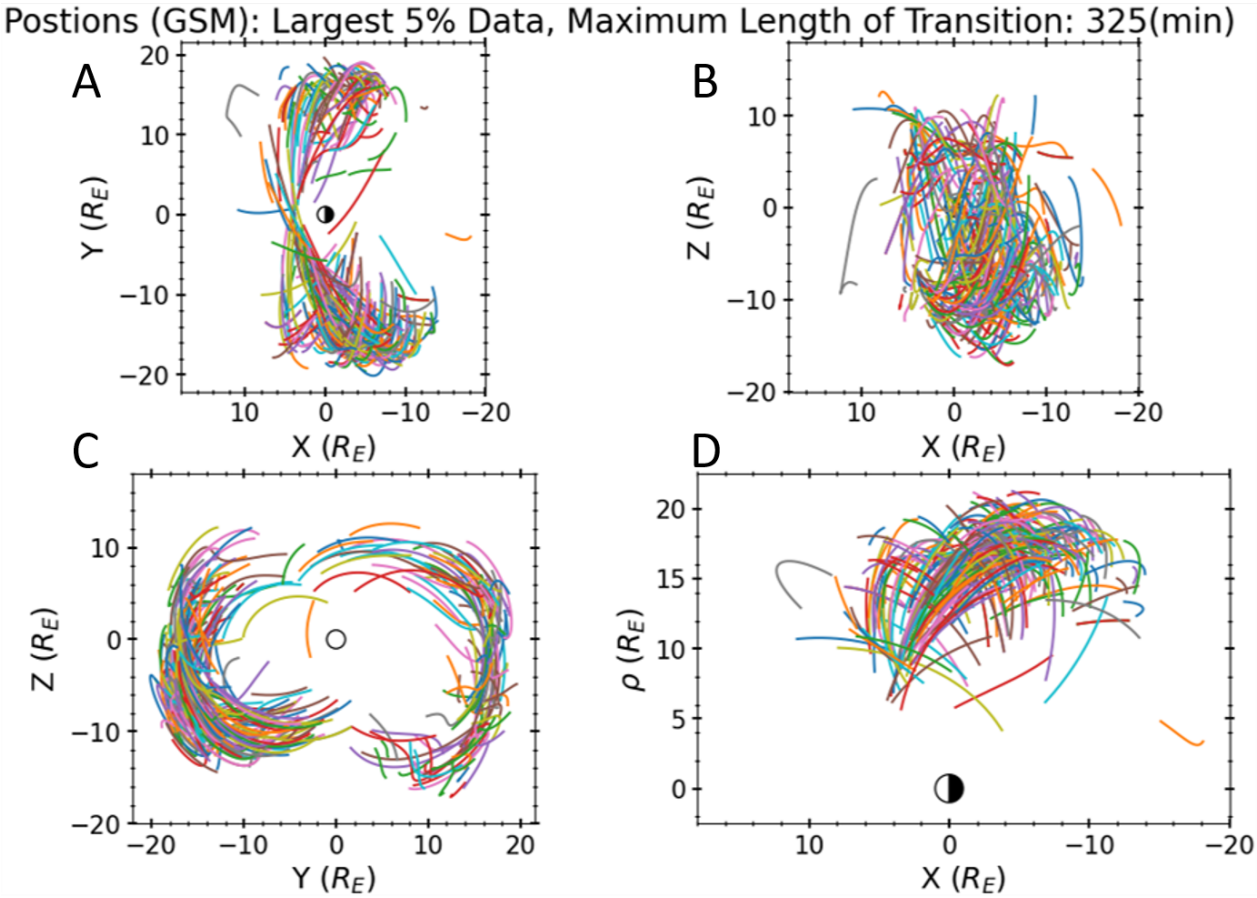

Figure 3.3: Positions of the longest 5% of crossings, based on time Cluster takes to cross, in GSM coordinates. Panel A shows the X-Y plane, panel B shows the X-Z plane, panel C shows the Y-Z plane, and panel D shows the X-ρ plane

Some of the longer magnetopause crossings found within the GRMB dataset are shown in figure 3.3 where the positions of the longest 5% of crossings are represented in GSM coordinates. This also displays the irregular orbital patterns (compared to GSE coordinates)

found if observed within GSM coordinates, caused by the movement of the axes. Similar patterns in the orbital paths as shown in figure 2.5 can be seen in figure 3.3. The paths shown within figure 3.3 are less structured than the ones found in figure 3.2. This is a product of the graphs produced in GSM coordinates, and the extreme nature of the longer crossings, most of which are longer than predictions suggest.

3.3 Model Comparison

To compare the Cluster data to a magnetopause model a common variable has to be found. To find this variable, the X-ρ plane has been used. Taking a crossing of the magnetopause found by Cluster would create a line where the magnetopause is predicted to be; finding the midpoint of this line gives the most probable location of the magnetopause for that crossing. This produces the Cluster points in figure 3.4, shown in red. The average Shue model can then be found using the input values $\alpha = 0.612$ and $r_0 = 10.161\,R_E$, taken from Shue *et al.* (1997), shown in blue. There is a similar trend shown between the data and the model, except with an overestimation by the model compared to the data at the highest θ values found by Cluster. The Cluster data is found in a wide area around the average Shue model, as the magnetopause measured will be influenced by the solar wind conditions, as explained in section 1.1.1.

By taking the midpoints of the Cluster crossing and converting the Cartesian coordinates to polar coordinates, an angle and radius can be found to represent each magnetopause crossing location. This process is shown in figure 3.5. Taking the Solar Wind conditions at the time each Cluster data point is found, as the input to the Shue *et al.* (1998) model equations, allows a predicted magnetopause to be drawn for every Cluster point found. Using the angle found for the Cluster data point, a line can be drawn to the predicted Shue magnetopause, giving a radius value for the Shue model; shown as the blue arrow on figure 3.5. With all of this combined, there are two radius values at a specific angle, for the Cluster data point and the predicted model, using the specific solar wind conditions at that time. This method is used to provide a consistent angle between the Cluster point and the model point, allowing the analysis of how the difference between the two models develop from the nose of the magnetosphere to the magnetotail. The distance between the Cluster magnetopause crossing and the location of the modelled magnetopause along the same radial line can be used to assess the accuracy of the Shue model.

3.3.1 Overall Comparison

Using the method outlined in the previous section, the angle (θ) against the difference in radii can be plotted, shown in figure 3.6 as the blue points. The Y axis is the difference in radii divided by the radius of the predicted model, giving the fractional difference between

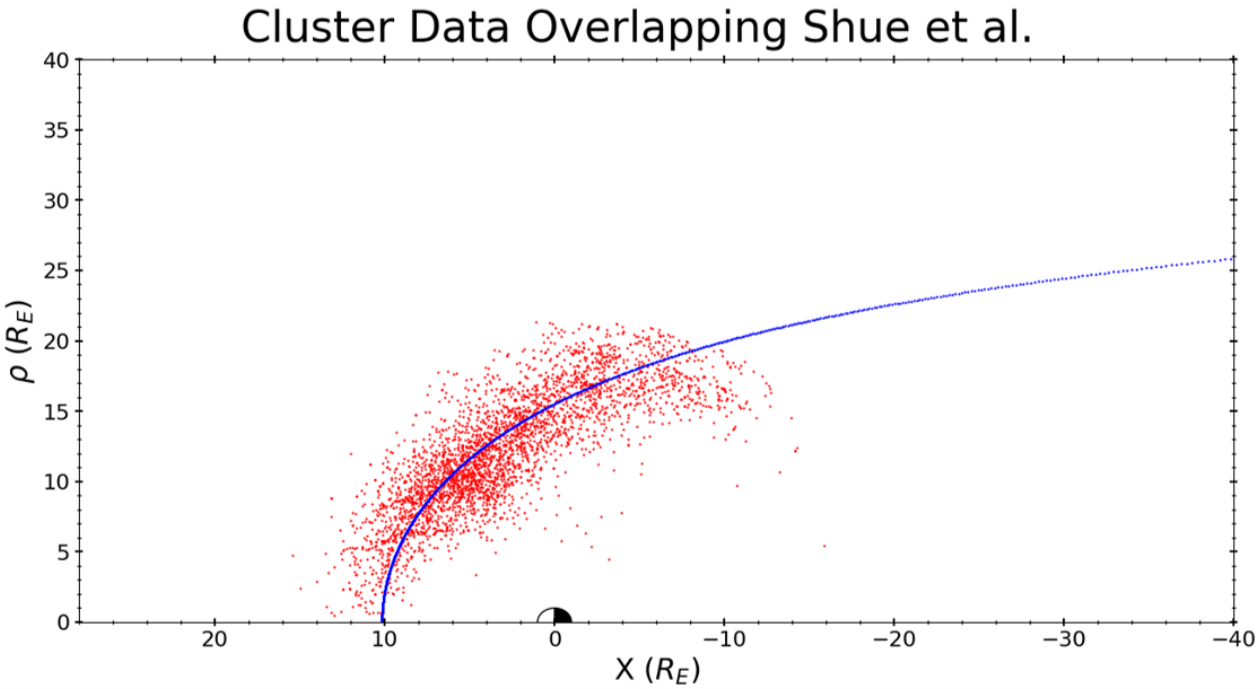

Figure 3.4: The average Shue model using $\alpha = 0.612$ and $r_0 = 10.161\ R_E$ input values (shown in blue), with the Cluster 1 data overlapped (shown in red). These Cluster 1 points are the midpoints in the X-ρ plane for 50% of the shortest magnetopause crossings, to find the most probable location the magnetopause is in. The motion of the magnetopause is accounted for in the GRMB dataset with the use of the transition region, and will unlikely affect the 50% shortest crossings

the radii. This is again for the shortest 50% of crossings based on the time Cluster is within the magnetopause region. The motion of the magnetopause is accounted for by using the magnetopause transition region within the GRMB dataset, as the periods of rapid crossings that would be found with a moving magnetopause are all counted as one crossing.

It is important to see how the distribution of points changes as the angle θ increases. To do this the data has been binned every 10%, this is due to the large grouping of data typically between 40° and 100°. There was consideration of binning the data based on width determined by degrees in θ, however, this produced large differences between the standard deviations. This isn't inherently problematic, but impaired the readability of the graphs, and the information the varying standard deviations provided can be seen by observing the width of each bin when using a percentage bin. The mean values of the bins are then plotted with a line connecting them, to see how the average changes dependant on the angle. The standard deviation of these bins are then found, to find the upper and lower limits of the uncertainty

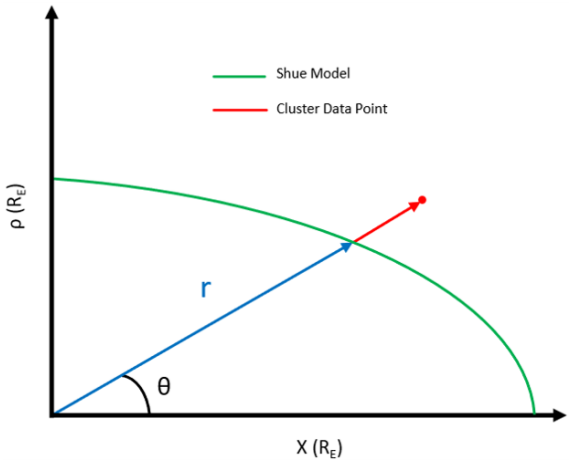

Figure 3.5: Diagram showing the calculation to compare between Cluster data and a model. This is done in the X-ρ plane, where each midpoint of a Cluster crossing is converted to polar coordinates, shown in red. An average Shue model is shown in green at a specific B_Z and D_P. Taking the angle at which the Cluster point is found and drawing a line to the model gives the blue line, where the r value of the model is found. Then the model r value can be taken away from the Cluster r value to compare the difference, which will then be divided by model r value to give a percentage difference

for each mean point. This upper and lower limit is then plotted with a green dotted line, above and below the mean line, showing the uncertainty and how that changes as the angle θ increases. This region is shaded in blue, to highlight further how this uncertainty changes.

Figure 3.6 shows that at low angles (near the nose of the magnetopause) the Shue model underestimates compared to the Cluster data by around 10%. Extrapolating back to the lowest angle value, the average at this point shows a larger underestimation, closer to 20%. This difference decreases as the angle increases (the further towards the magnetotail), until 40° where the Shue model agrees with the data found. This remains relatively consistent (within 4% of the Cluster values), until about 105° where the Shue model starts to overestimate compared to the data, which is explained in section 3.4.

3.3.2 Percentage Investigation

It is important to understand what proportion of the data can be trusted, for the correct balance of uncertainty and number of data points, as we have seen many irregular crossings from the GRMB dataset. The magnetopause can be found anywhere within the magnetopause crossing region, at which the location may vary on a short enough timescale to be measured more than once during a Cluster crossing. This causes uncertainty as to where

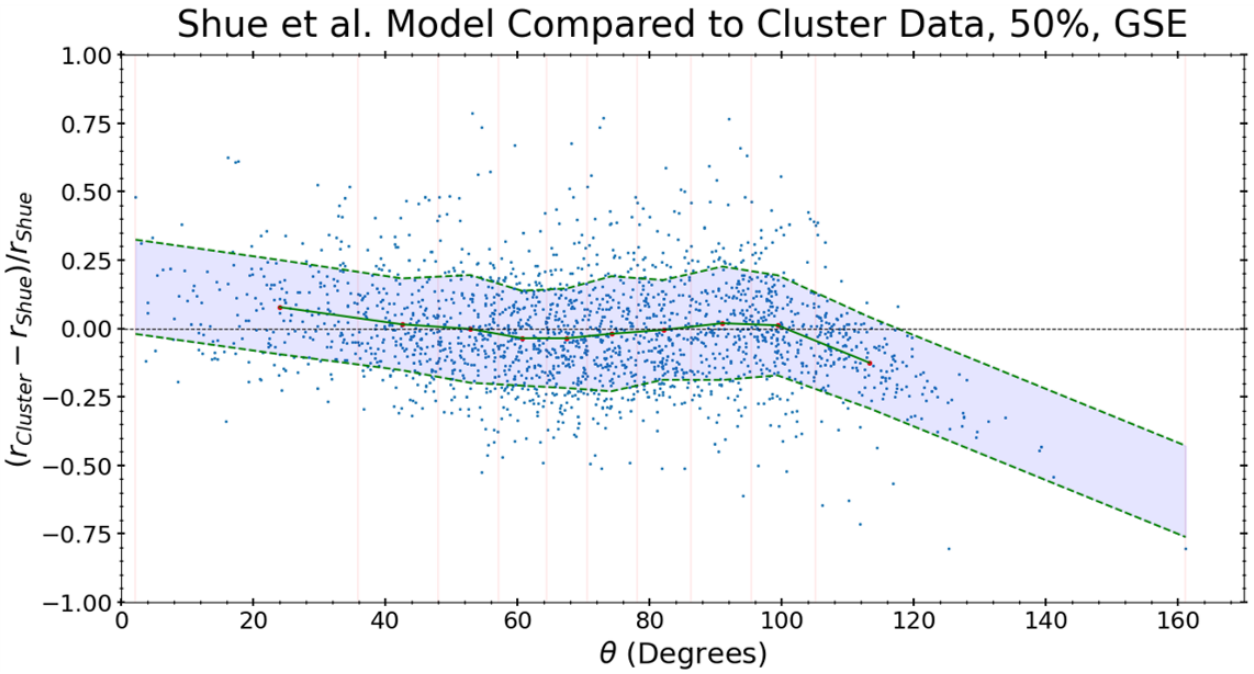

Figure 3.6: Comparison between the Cluster data and the Shue model r values as angle θ increases. This is for shortest 50% of magnetopause crossings in GSE coordinates. Every 10% of the data, as the θ value increases, is binned with the averages and standard deviations of these bins calculated and plotted. This gives the average line plotted in green with red points, and the standard deviation above and below the average plotted with the green dashed lines, with the blue shaded region between

in the region identified by the GRMB dataset the magnetopause is located. Now that an initial comparison has been made using the shortest 50% of these magnetopause crossings, the proportion of trusted data can be found. For this a cumulative distribution function of the distance covered in these crossings can be compared to the uncertainty in figure 3.7, once it has been converted to Earth radii.

The standard deviation for each of the angle bins found in figure 3.6 has been calculated, representing the uncertainty in the average values of these bins. This however, is a dimensionless uncertainty, so to convert this to a distance, the average Shue radius has to be determined. The calculation of the Y axis in figure 3.6 involves dividing by the Shue radius to determine the fractional difference between the model and data. For this 50% sample of the data, the average Shue radius is 14.241 R_E, and the average standard deviation is 0.183. This gives a 2.6 R_E uncertainty. The average Shue radius calculated here is significantly different to what is predicted for the standoff distance within Shue *et al.* (1997). This is a result of the radius value of the magnetopause increasing as the θ value increases, as the distance to

the magnetopause will be much larger at the magnetotail than the nose of the magnetopause. The average calculated here is an average for all θ values of the Cluster data points.

This uncertainty can now be used to determine the percentage of events that can be trusted to provide the location of the magnetopause. For this, the average change in distance for each of the crossings can be found. This is done by integrating each crossing event to determine the total distance travelled by Cluster. By repeating this process for all the crossings, a cumulative distribution function of the crossing distances can be created, to show how many of the crossings are within this $2.6\,R_E$ found. This is represented in figure 3.7.

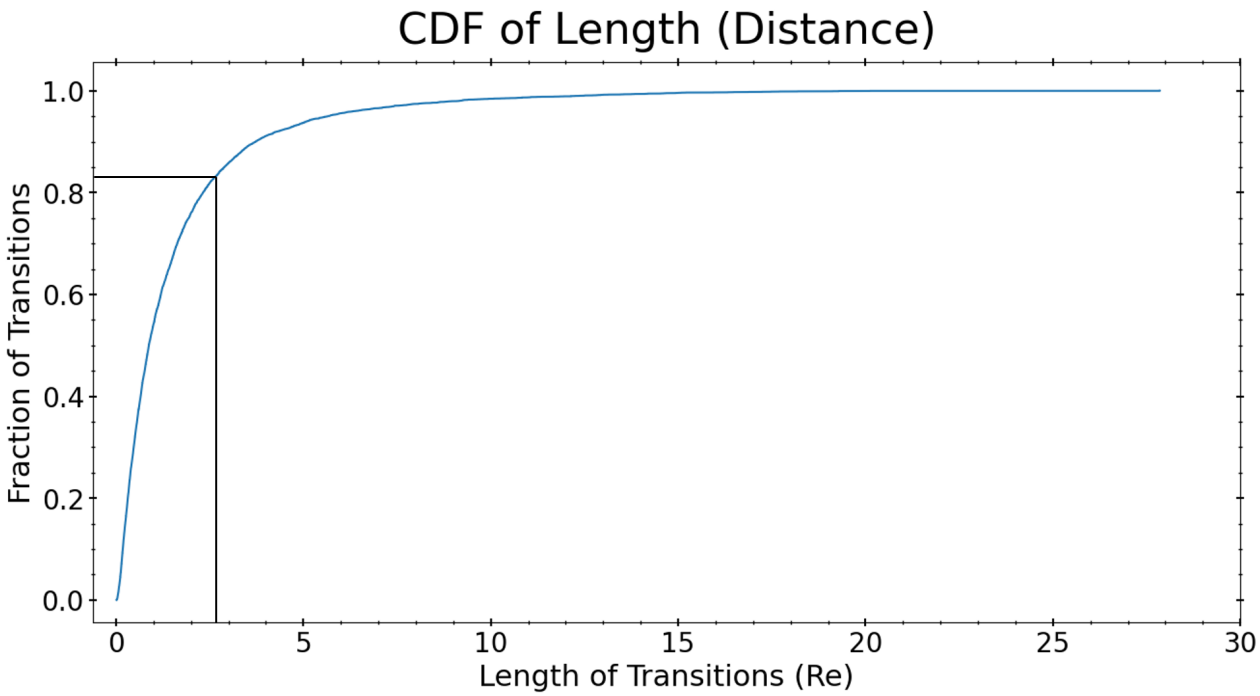

Figure 3.7: Cumulative distribution function showing how the distance travelled during a crossing accumulates based on the proportion of data. This allows the analysis of the optimal percentage of the data to use, by using the average standard deviation in figure 3.6 in R_E as the input in the X coordinate, and finding the Y coordinate

83% of magnetopause crossing events have a transition length of $2.6\,R_E$ or less. This is roughly 80% (126 minutes), which will be used as the basis for further analysis.

3.3.3 GSM Co-ordinates

3.3.3.1 GSM Positions

Figure 3.8 is a representation of the overall comparison between the Shue model and Cluster data using 80% of the data, in GSM coordinates. When comparing this to the GSE coordinate version, there is no variation in points or averages. The subtle differences shown between figure 3.6 and figure 3.8, are caused by the difference in the percentage of the data analysed. This is the expected outcome, since both the Shue model and the Cluster data points will be shifted by equal proportions when changing from GSE to GSM coordinates. The differences between GSE and GSM will arise when latitude and local time restrictions are imposed, as these one-dimensional restrictions will be shifted. The two main differences that can be found between the 50% and 80% graphs are, the small overestimation by the Shue model at 55°, and the 75° point estimating closer to the Cluster data, for the 80% graph.

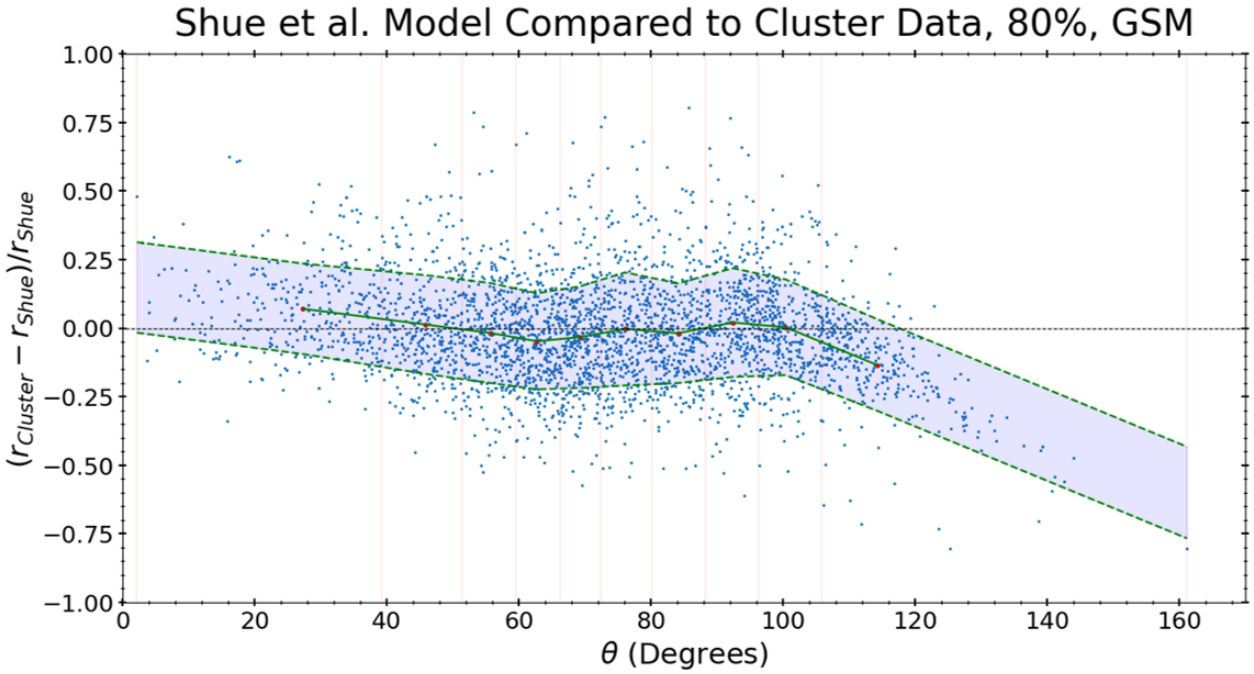

Figure 3.8: Comparison between the Shue model and Cluster data as angle θ increases. This has been done for 80% of the crossings in GSM coordinates. Every 10% of the data, as the θ value increases, is binned with the averages and standard deviations of these bins calculated and plotted. This gives the average line plotted in green with red points, and the standard deviation above and below the average plotted with the green dashed lines, with the blue shaded region between

3.3.3.2 Latitude Variation

It is useful to see how the comparison between the Shue model and the Cluster data changes under certain parameters. One of these parameters can be the latitude at which the measurements are taken. This explores how the shape of the magnetopause changes, the further North (or South) the measurements are taken. The latitude is calculated using equation 3.1.

$$Latitude = \arctan\left(\frac{Z}{\sqrt{X^2 + Y^2}}\right) \tag{3.1}$$

Using this, figure 3.9 is produced, showing the latitudes comparison for 80% of the data. Figure 3.9 shows a comparison between 0° to 30° latitude and 30° to 60° latitude. The 0° to 30° latitude graph shows that the Shue model consistently underestimates the radial location of the magnetopause by about 10% for all θ values. However, for the 30° to 60° graph, the model slightly overestimates compared to the data, between 50° and 90°. For the rest of the θ values the model and the Cluster data roughly agree. This shows that the Shue model predicts a smaller magnetopause at the nose of the magnetosphere, due to the consistent underestimates between 0° and 30° latitude. The lowest θ in the latitudes 30° to 60° graph is 30°: since the angle θ will increase as either the latitude or the angle between the X and Y axes increase. Therefore, with 30° being the lowest the latitude can go, the θ value will not go below 30°.

Figure 3.10 shows the comparison between Cluster data and the Shue model for latitudes between 60° and 90°. There is less data in the 60° to 90° graph, likely arising from the lack of mission time in the necessary region to encounter the magnetopause, due to the size of the magnetopause in this region commonly stretching beyond Cluster's orbit. However, figure 3.10 shows that the Shue model consistently overestimates in this region by approximately 10% to 15%. This is a significant difference from the Cluster data, larger than that of the lower latitudes, suggesting the Shue model is less accurate at measuring the magnetopause location at higher latitudes. This occurs since the Shue model is derived from data of satellites that only explored the lower latitudes.

3.3.3.3 Southern and Northern Hemisphere Comparison

The difference between the northern hemisphere and southern hemisphere can also be analysed using the Latitude calculated in equation 3.1. The magnetopause shape differs between the northern and southern sections of the magnetosphere, caused by Earth's dipole tilt. This produces an interesting comparison between a symmetrical model, such as the Shue model, and the measured representation of Cluster.

In figure 3.11, there are slight differences between the northern hemisphere and the southern

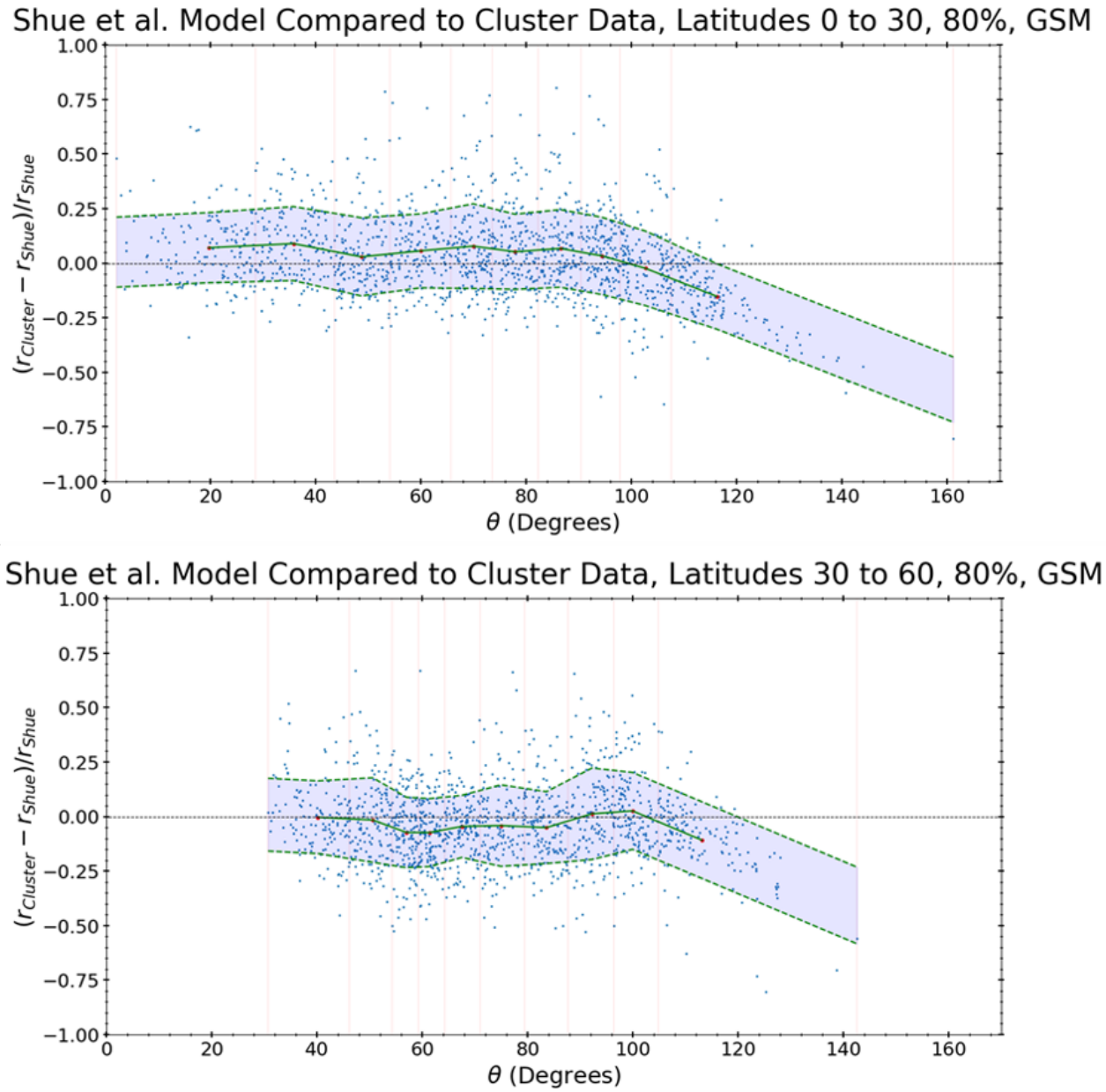

Figure 3.9: Comparison between the Cluster data and Shue model as angle θ increases. This is done for 80% of the crossings, in GSM coordinates, with crossings between latitudes 0° and 30° for the top graph and latitudes 30° and 60° for the bottom graph

hemisphere. Both hemisphere averages start with around a 5% to 10% underestimation by the Shue model compared to the Cluster data. The extrapolation of the southern hemisphere's average suggests a larger underestimation at the very lowest of angles. By

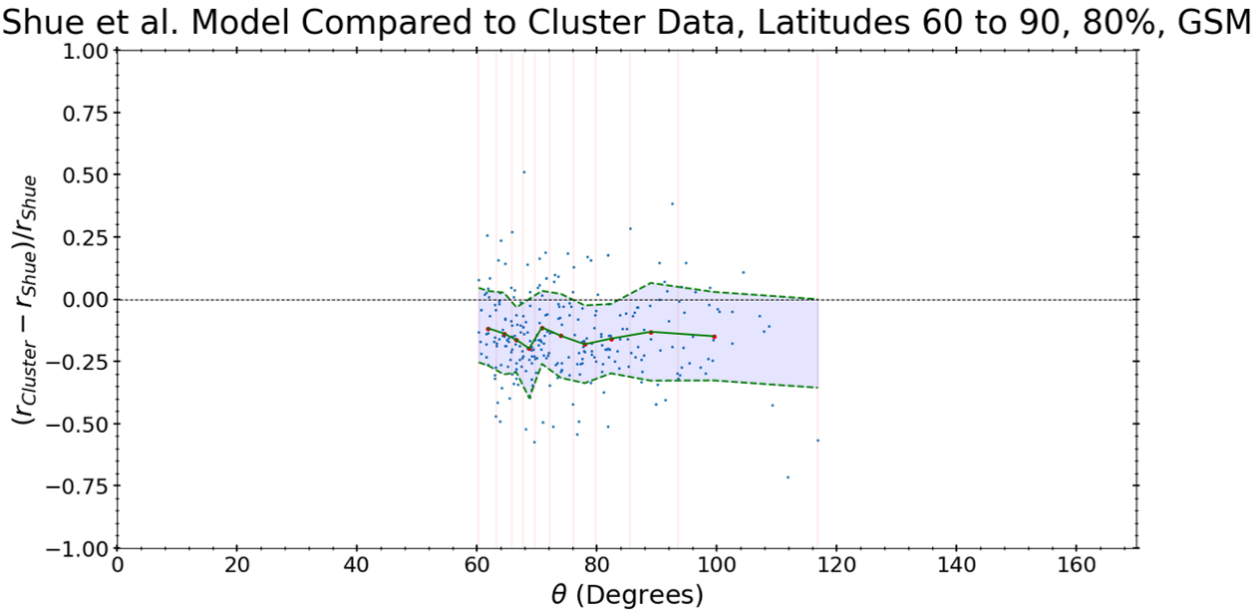

Figure 3.10: Comparison between the Shue model and the Cluster data as angle θ increases. This is for 80% of the crossings, in GSM coordinates, between latitudes 60° and 90°

around 45° the model agrees with the northern hemisphere data, before reaching 100°. The southern hemisphere is more variable though, with the underestimation turning into a slight overestimation by 60°. This then changes into an underestimation by 100°. Overall, it can be seen that the southern hemisphere magnetopause is closer to Earth than the northern hemisphere, with a more varied structure. To understand this observation the structure of the Shue model has to be considered, in which it is a symmetrical model between the northern and southern hemispheres. This suggests that a symmetric model does not accurately reflect the magnetosphere's north-south asymmetries. This is likely a result of the dipole tilt angle found with Earth's magnetic field, as this will cause the magnetic field strength to be different at similar points in latitude and local time between the southern and northern hemisphere. However, the seasonal bias of Cluster between the start of the mission and 2010 may have a factor in the differences seen between the northern and southern hemispheres.

3.3.3.4 Local Time Variation

Local time represents the relative position to the Sun of a particular point around a planet, using 24 hours as a full rotation, starting at midnight the opposite side to the Sun. For the purposes of this analysis, local time can be calculated using equation 3.2.

$$Local\ Time = \arctan\left(\frac{-Y}{-X}\right) \cdot \frac{24}{2\pi} \tag{3.2}$$

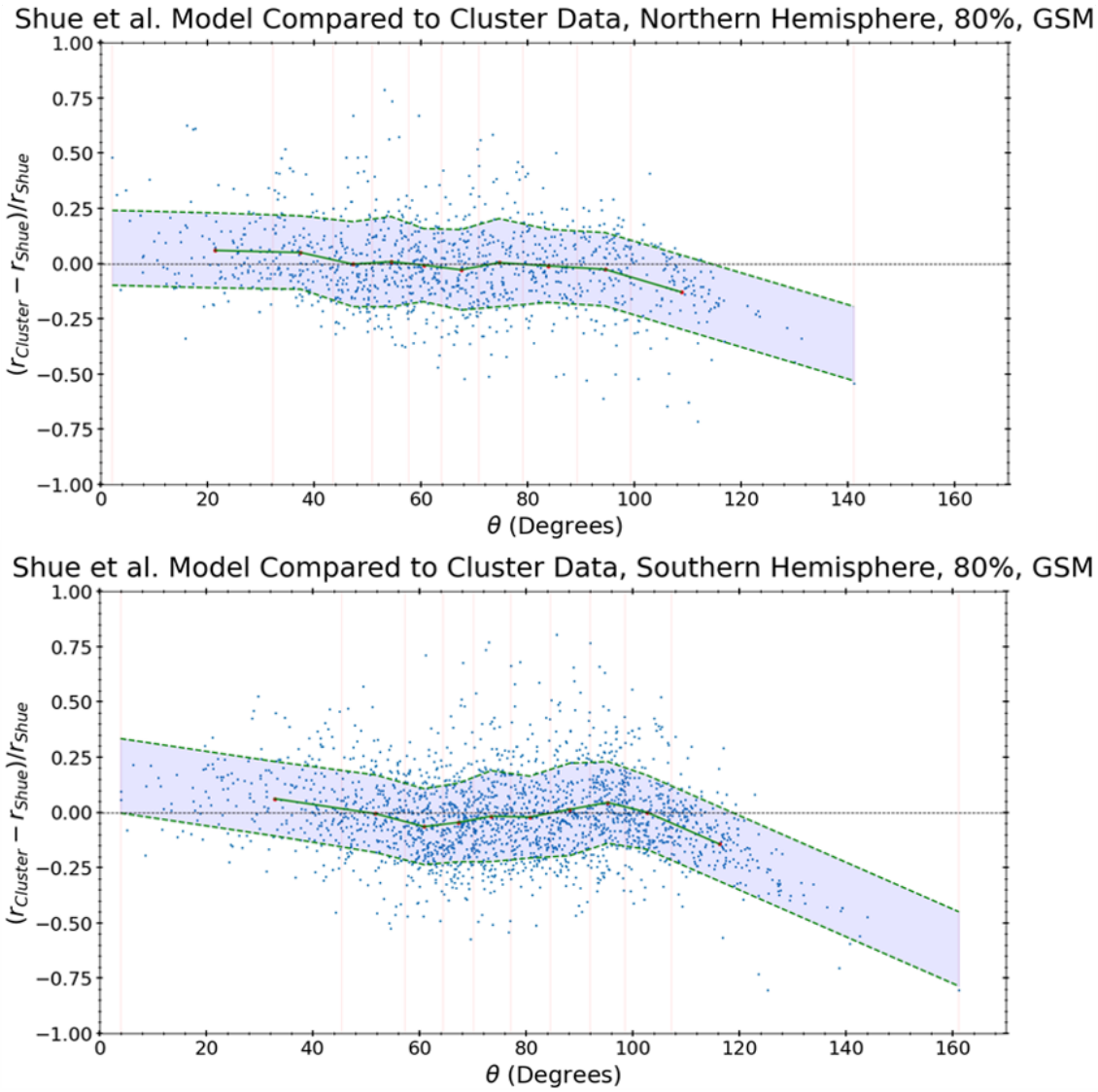

Figure 3.11: Comparison between the Shue model and Cluster data as angle θ increases. This is for 80% of the crossings, GSM coordinates, with the top graph showing the northern hemisphere and the bottom graph showing the southern hemisphere

This can then be split into 4 quadrants to represent the different sections of local time: 0 to 6 hours is the dawn quadrant, nightside. 6 to 12 hours is the dawn quadrant, dayside. 12 to 18 hours is the dusk quadrant, dayside. 18 to 24 hours is the dusk quadrant, nightside. Using local time as a limiting factor allows analysis of the solar wind compression effect between the nose of the magnetopause and the magnetotail. Additionally, the difference between the

dawn and dusk sides of the magnetopause can be analysed (taking the Earth-Sun line as the midpoint).

Figure 3.12 shows the four quadrants for 80% of the crossings. A similar effect to that observed with latitude limiting the θ angle can be seen, where the nightside measurements start at 90°. This occurs for the same reason, as for the measurements to be on the nightside, they have to be above 90° in latitude limiting the θ angle to 90° and above. In reality, the latitude would start to decrease, with the angle between the X and Y values increasing further.

For the nightside graphs, the model and the data seem to largely agree, with larger variability for the local time 18 to 24 graph, compared to the 0 to 6 graph. Local time 6 to 12 starts with the Shue model underestimating the location of the magnetopause by approximately 5%. By about 50° the model and the data largely agree, until 90° where the limit described in the previous paragraph takes effect. Local time 12 to 18 is more variable than local time 6 to 12, with the average value starting at a 10% underestimation by the model. This then decreases to the point where the model and the data almost agree with each other by 40°. Between roughly 50° and 75° the Shue model overestimates by at most 10%, then from 75° to 90° the model and data roughly agree. Overall, the dusk side of the magnetopause has a more varied structure according to the comparison between the Shue model and the Cluster data, but with both the model and data close to agreeing for the majority of each local time quadrant.

3.4 Sampling Bias

Throughout all of the comparison graphs, between the Shue Model and Cluster data, there has been a substantial increase in the overestimation by the model at the largest of θ values. This was initially an unexpected behaviour that needed to be investigated.

For this, the investigation started with how often the Cluster data points were found outside some Shue models with varied solar wind conditions. The Cluster data was then overlapped on top of these models. This was an attempt to give a visual interpretation of how often Cluster is found outside the predicted magnetopause models, as the model progresses towards the magnetotail.

To produce the Shue models the OMNI solar wind data is used by sorting the dynamic pressure and IMF B_z, at the times used for all the Cluster data points, in order of increasing values. Then every 10% increment of the dynamic pressure and B_z are found, giving a list of eleven numbers representing these 10% increments. The largest and smallest values are then removed as they create far too extreme of values. Both of the lists created are then paired with a typical value for the other variable (e.g. the incremented list for dynamic pressure

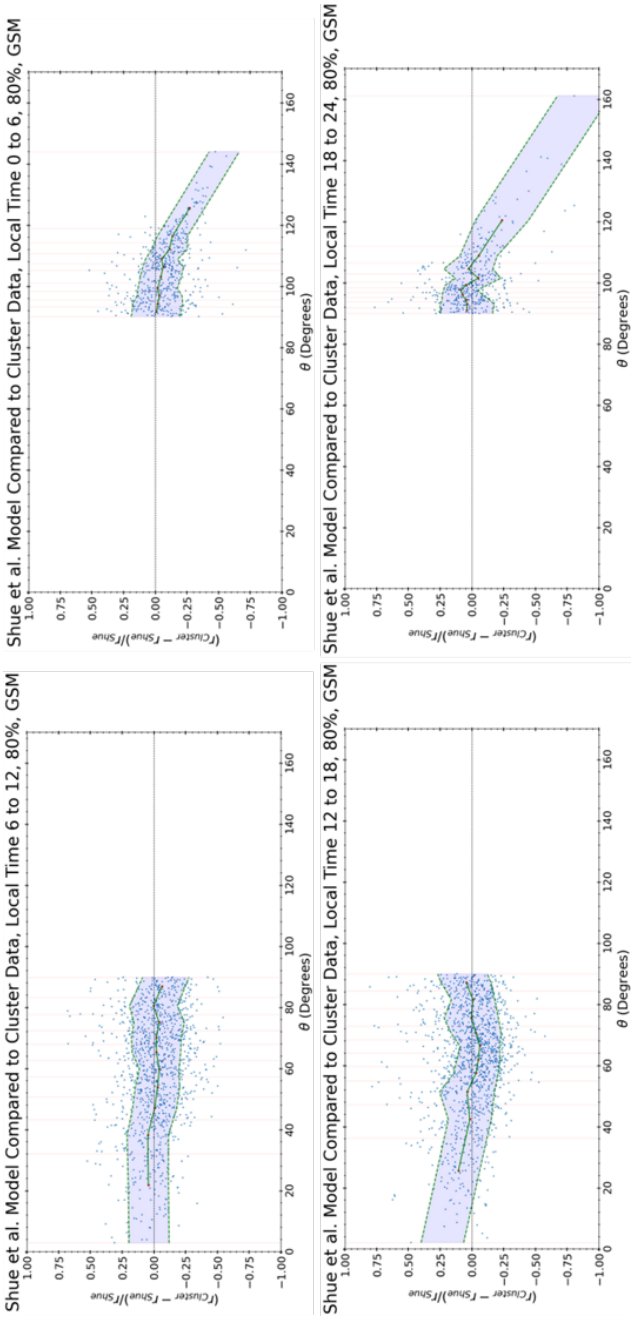

Figure 3.12: Comparison between the Shue model and Cluster data as angle θ increases. This is for 80% of the crossings, GSM coordinates, restricted into local time quadrants. The bottom left is local times 6 to 12, the top left is 0 to 6, the bottom right is 12 to 18, and top right is 18 to 24

paired with an unchanging B_z). This gives two sets of magnetopause predictions with a changing solar wind variable, when used with the Shue model.

In figure 3.13 the predicted magnetopauses found have been plotted over the positions of the Cluster magnetopause crossings. The Cluster magnetopause positions were found from the midpoints of 80% of the crossings given by the GRMB dataset; the midpoints give the best idea of where the magnetopause might be. It can be seen that an increase in IMF B_Z results in a slightly larger standoff distance to the nose of the magnetopause, but a much smaller magnetopause towards the magnetotail. With an increase in dynamic pressure, the magnetopause compresses along all points on its surface. This only gives a visual representation though, which is insufficient to find the point where the data can no longer be trusted due to the sampling bias, a more quantitative method will need to be found.

Finding what quantity of Cluster points that are outside the Shue model involves finding the average prediction of the magnetopause based on Shue, using the average Solar wind conditions. This is using a similar method used earlier to find the comparison graph in section 3.3.1, for the entire Cluster mission. Grouping the data based on angle (θ), the proportion of these groups that are outside the predicted magnetopause can be found. This is to see how often Cluster is outside the magnetosphere for a given region. This gives figure 3.14.

Figure 3.14 shows that with low θ (near the nose of the magnetosphere), more than 80% of the time Cluster is outside the Shue magnetopause prediction. This continues until about 30° where the time Cluster spends outside the magnetopause reduces at an increasing rate. This sharply levels off at around 70° and 50%, before the time outside the magnetopause again reduces at an increasing rate. At around 120°, Cluster is no longer found outside the magnetopause, as none of the measurements are found outside the prediction.

Using similar methods, the time Cluster spends near the predicted magnetopause can be found. For this a $4R_E$ width band around the predicted magnetopause is considered. This can be done to analyse the zone within the magnetopause, and outside the magnetopause, represented in figure 3.15.

Outside the magnetosphere starts with a higher percentage at around 5%, compared to 3% for inside the magnetosphere, suggesting Cluster spends more time outside the magnetosphere. Between 5° and 65° the apogee of Cluster's orbit will be much larger than the distance to the magnetopause, resulting in Cluster spending more time outside the magnetosphere and therefore will be more likely to be found outside. There is a small period of time where Cluster is more often found to be inside the magnetosphere, about 65° to 75°, this will be where Cluster starts to spend more time inside the magnetosphere than outside. Then

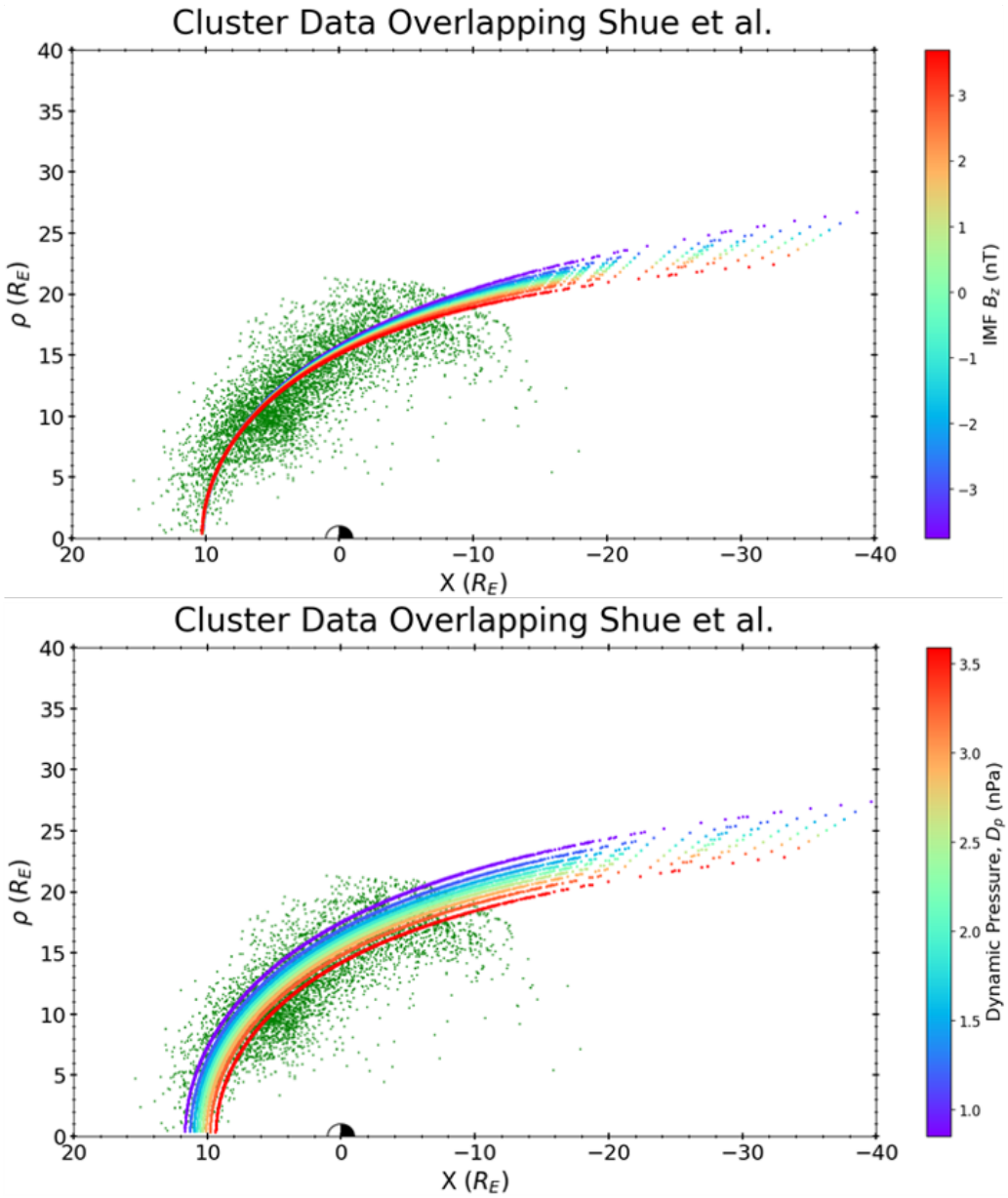

Figure 3.13: Average Shue models overlapping Cluster data from the midpoints of the X-ρ graph in figure 3.6. Each Shue model is plotted by finding all the IMF B_Z and D_p values that pair with the Cluster data times, ordering them, and creating a list out of every 10% increment of the data. These lists are then paired with an unchanging value of the other variable, to give a set of magnetopause predictions. The top graph is made with a fixed D_p and a variable B_Z, the bottom graph is made with a fixed B_Z

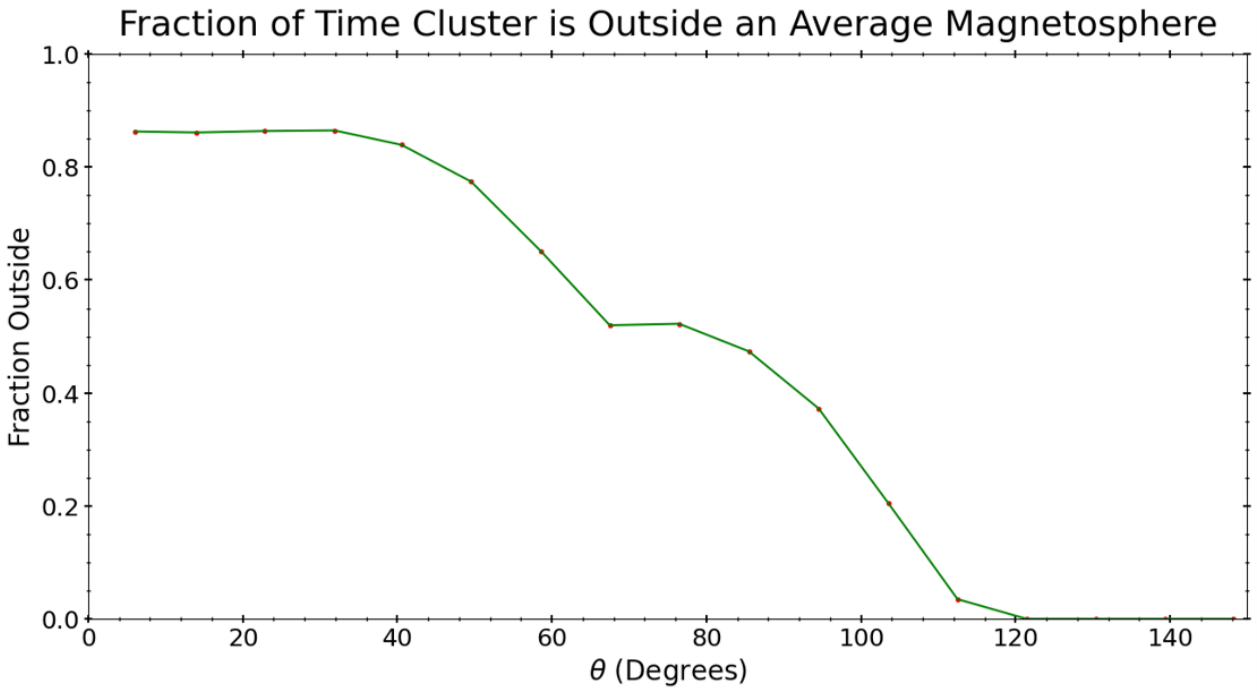

Figure 3.14: The proportion of Cluster data points that are outside an average Shue model, as angle θ increases. This shows how often Cluster is expected to be outside the magnetopause

between 75° and 100° Cluster is more likely found just outside the magnetopause. This is where Cluster will be skimming the magnetopause and therefore spend long periods of time just outside the magnetosphere, before quickly returning towards perigee, spending less time just inside the magnetosphere. By 100°, Cluster's orbit will be almost entirely inside the magnetosphere, therefore Cluster is more likely to be found within the magnetosphere and will spend a higher proportion of its time there. By 120° Cluster is no longer outside the magnetopause, and by 130° Cluster isn't found near the magnetopause.

From these results, it appears that the potential sampling bias starts to take effect at 100°. This conclusion can be made as Cluster is found progressively more within the magnetosphere, not even coming close (within $2\,R_E$) to the predicted magnetopause boundary by 130°. This causes less reliability of the data from 100°, since Cluster won't be found in the necessary area to measure the magnetopause under normal conditions. Therefore, only the highly compressed magnetospheres, with stronger solar wind conditions, will be measured. This may cause the average value of the magnetopause position to be smaller according to Cluster, but will also come with a more compressed magnetopause surface from the Shue model, diminishing this potential Cluster sampling bias. This suggests the predictions and measurements can not be trusted beyond this region.

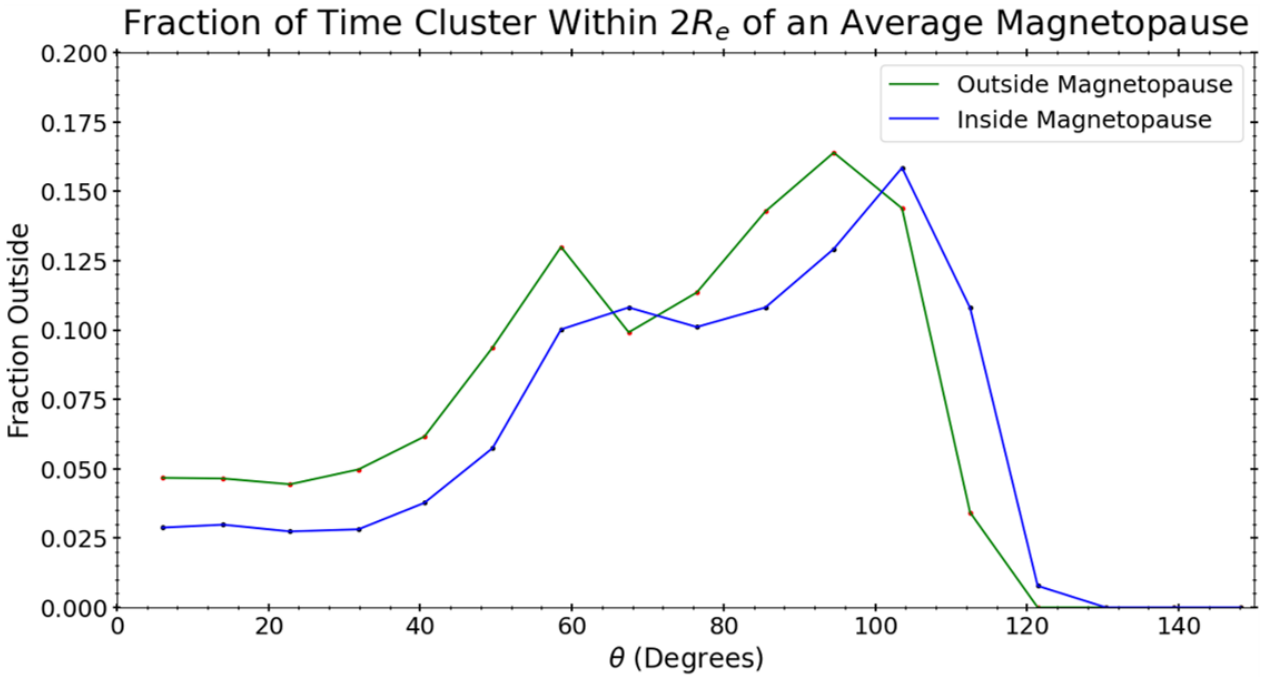

Figure 3.15: The proportion of Cluster data points within $2\,R_E$ bands inside and outside the average Shue magnetopause. This shows how often Cluster is close to the magnetopause and which side of the magnetopause, and therefore how often Cluster is able to take measurements of the magnetopause

Despite the investigation into potential Cluster sampling bias, some consideration has to be given to the inaccuracies of the models, as the Cluster sampling bias isn't a perfect explanation. The previous paragraph has shown that the Shue model won't predict the magnetopause well in regions beyond 100°. This is likely due to the Shue model using data from low latitude satellites. It will be seen in section 3.5 that the Lin and Liu models also have a similar affect beyond 100° when compared to the Cluster data. Seeing as the Lin model uses data from Cluster, this would suggest there is more than just Cluster sampling bias that may cause this shift towards an overestimation by the models. This idea is amplified by the models having different overestimations of the magnetopause location beyond 100° of θ in the latitude 60° to 90° graph; figure 3.19 in section 3.5.2. Overall, there is evidence for Cluster sampling bias to be responsible for the overestimation by the models, seen when comparing the models with the Cluster data beyond 100°; however, this may not be the only cause for this affect when considering the nature of the models.

3.5 Asymmetrical Models

3.5.1 Overall Comparison

A comparison between the Cluster data and the models can be made. This is done using the same method as with the Shue model described in section 2.5.1, then plotted in section 3.3.1. The difference in distance is still measured radially from Earth within the cusp region introduced by the asymmetrical models, this can be seen in figure 3.16. This will give three separate comparison graphs that can be overlapped, to give a comparison between each model and the Cluster data.

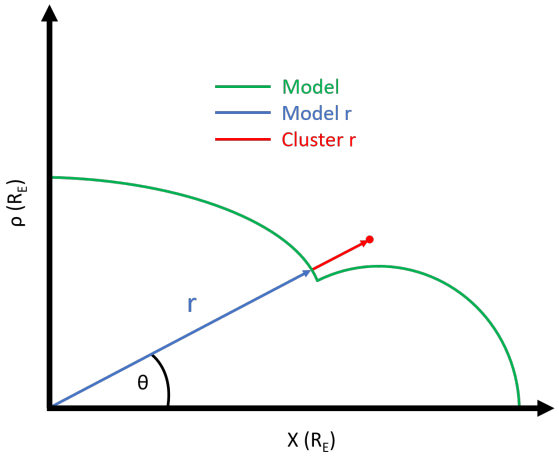

Figure 3.16: Diagram showing the calculation to compare between Cluster data and a model. This is done in the X-ρ plane, where each midpoint of a Cluster crossing is converted to polar coordinates, shown in red. An example model is shown in green. Taking the angle at which the Cluster point is found and drawing a line to the model gives the blue line, where the r value of the model is found. Then the model r value can be taken away from the Cluster r value to compare the difference. This is shown as an example for how the difference is calculated in the cusp region

Figure 3.17 gives an unrestricted view of the comparison between the cluster data and the models. As previously analysed, the Shue model starts with an underestimation of the magnetopause location, then roughly agrees with the Cluster data, progressing to a section where the model overestimates compared to the data. The asymmetrical models consistently underestimate the radial location of the magnetopause, before reaching 100°, with the Liu model underestimating more than the Lin model. This is shown with the 76° average point showing an 8% underestimation for the Liu model compared to 4.5% underestimation for the Lin model. Overall, the asymmetrical models will tend to underestimate, and the Shue

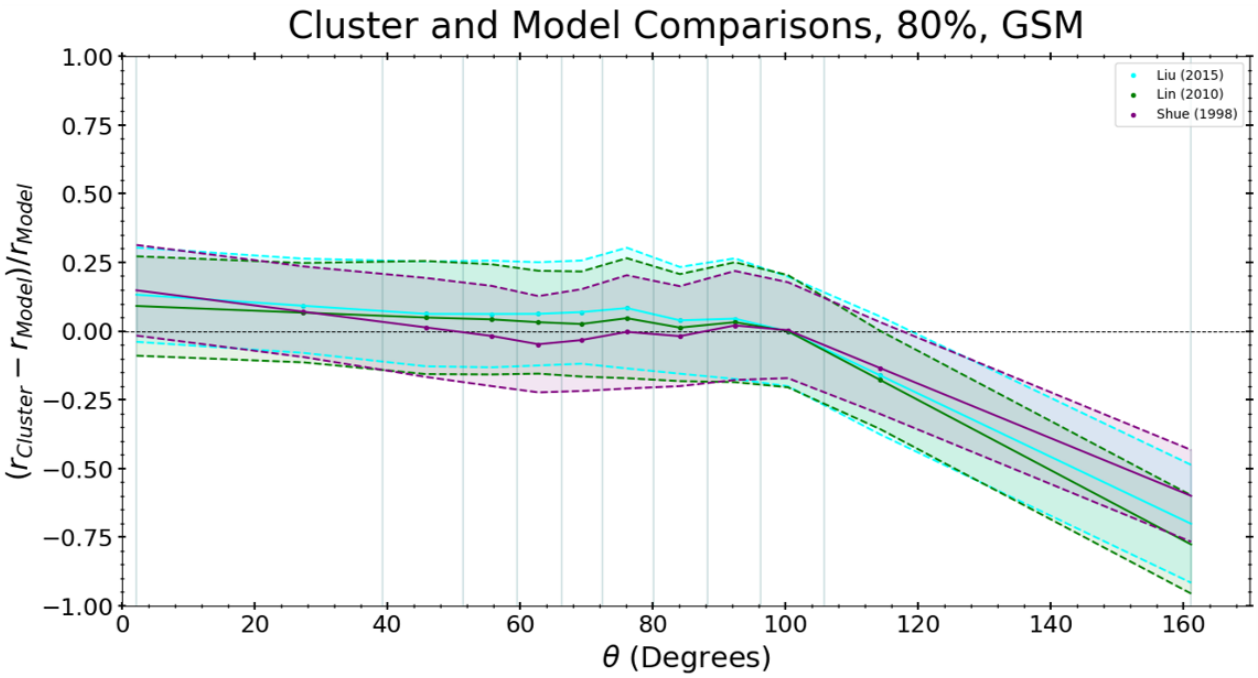

Figure 3.17: Comparison between the Cluster data and all three magnetopause models as angle θ increases. This is for 80% of the crossings in GSM coordinates. The averages and standard deviations of the 10% data bins are plotted for all three models. The data points have been omitted to improve readability

model will tend to agree with the Cluster data or overestimate the radial location of the magnetopause.

Between all three models, the average points are found at the same θ values since this variable is based on the Cluster data as an input into the models. This means all of the points on the graph have the same θ between the models, just a different fractional difference between the selected model surface and Cluster magnetopause location.

There is consistently an underestimation by the models towards the nose of the magnetopause. This has been seen in many of the comparison graphs with figure 3.17 included, and can be seen in figure 3.4 and the top panel of figure 3.13. There could be a number of causes for this, such as again the shape of Cluster's orbit and total mission time in certain areas of the magnetopause, with less information in the lower latitudes compared to the mid to high latitudes. Also, for lower solar wind dynamic pressures the Shue model no longer underestimates the magnetopause location in this region, as seen in the lower panel of figure 3.13, which would suggest that this underestimation is simply due to varied solar wind conditions. This ignores how the comparison graphs are created though, with each Cluster

data point using the solar wind conditions for that point in time. A focussed study into this effect would be valuable to ascertain its true cause.

3.5.2 Latitude Variation

Again, it is important to investigate the difference between model and data within different frames, starting with a variation in latitude. Latitude is calculated in the same way as in section 3.9 for all the points found for the three models, to identify what data points are within the latitude range.

Figure 3.18 shows the 0° to 30° and 30° to 60° ranges for these comparisons. The 0° to 30° graph shows a similar trend between all three models when compared with the Cluster data. This trend is a relatively consistent underestimation by the models between 3% and 10%. This shows that at low latitudes the models all closely agree with each other.

For the 30° to 60° graph there is a larger variation between the models. The Shue model generally overestimates, with sections where it agrees with the Cluster data. The asymmetrical models both start by underestimating compared to Cluster, until about 55° where they start to disagree with each other. The Liu model roughly maintains the 5% underestimate of the magnetopause location until about 85° where it starts to agree with the Cluster data, before reaching 100° where the data may not be trusted. However, the Lin model agrees with the Cluster data from 55°, with a slight underestimate of magnetopause location, before reaching 100°. The asymmetrical models have a more accurate prediction of the magnetopause location compared to the Shue model in the mid latitudes.

For figure 3.19, where the 60° to 90° range is shown, there is a larger variation in the results. This will be caused by the differences with how the models have been made and the data that has been used. The Shue model struggles to predict the higher latitudes when compared with the asymmetrical models. This is shown with the significant overestimation of the magnetopause, varying around 15%. The differences between the Lin and Liu models likely arise due to the Lin being an empirical model, and the Liu model created using a magnetohydrodynamic simulation. These two methods can result in a significant difference when predicting an area with less data. The Lin model starts with a slight underestimation near 60° of 5%, this then moves towards an overestimation, reaching 13% by 100°. The Liu model starts with the 5% underestimation similar to the Lin model, however, the Liu model roughly maintains this underestimation until 82°. At this point there is a sharp trend towards an overestimation, reaching 32% by 100°.

The Shue model less accurately predicting the higher latitudes can also be seen, to a lesser

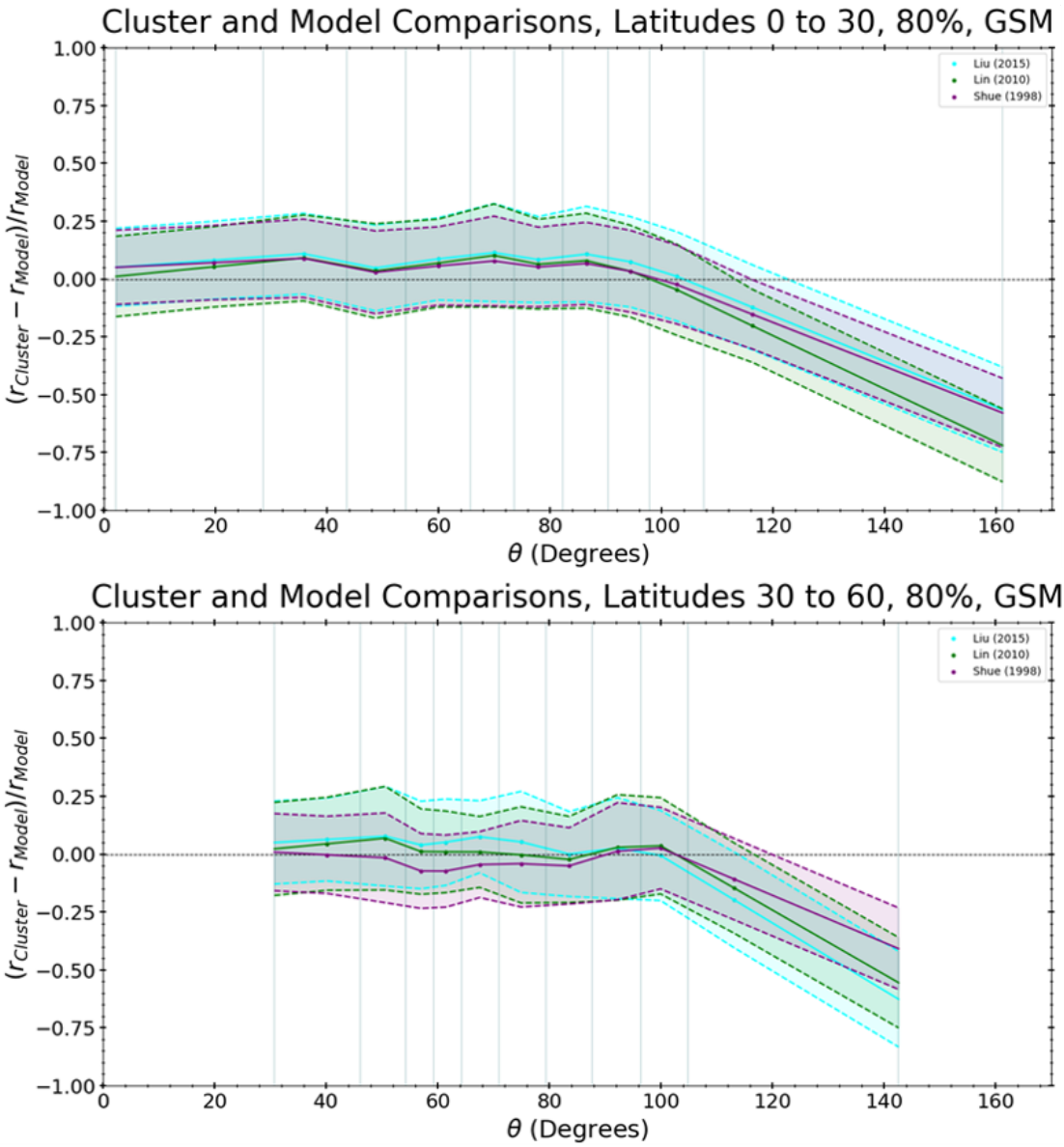

Figure 3.18: Comparison between the Cluster data and all three magnetopause models change as angle θ increases. This is for 80% of the crossings in GSM coordinates. The top graph shows the crossings between latitudes 0° and 30°, the bottom graph shows the latitudes 30° to 60°

extent, with the 30° to 60° graph as the Shue model deviates from the other models and the Cluster data. The data source of Shue may be to blame for this, as the missions used only explored the lower latitudes; whereas the two asymmetrical models used some Cluster data,

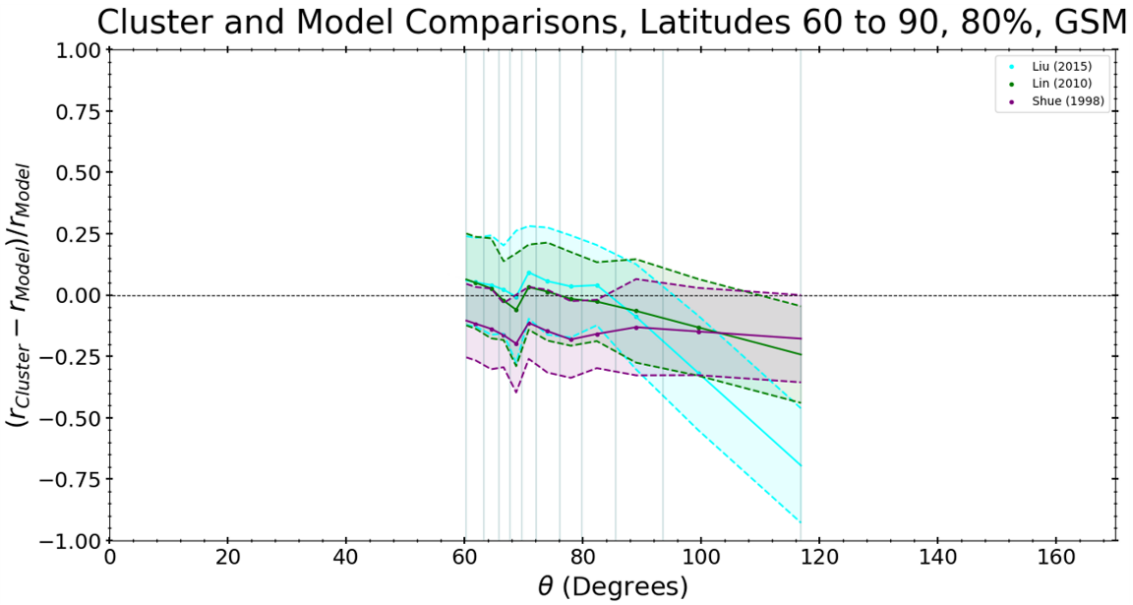

Figure 3.19: Comparison between the Cluster data and all three magnetopause models as angle θ increases. This is for 80% of the crossings in GSM coordinates. This shows the crossings between latitudes 60° and 90°

and predict the magnetopause better at higher latitudes. This suggests that the Shue model will have limitations beyond 30° latitude.

3.5.3 Southern and Northern Hemisphere Comparison

The cusp region can be more easily identified when looking at the northern and southern hemispheres when comparing the asymmetrical models with the Shue model. For this, figure 3.20 has been produced. Looking at the northern hemisphere the Shue model starts with a slight underestimation, then largely agrees, as described in section 3.3.3.3. Both asymmetrical models follow a similar trend, of a small underestimation varying within a 6% range before reaching 100°. However, the Liu model consistently underestimates a further 4% or 5%, the largest of underestimations occurring around 60°. This agrees with figure 2.11, where in the X-Z plane the Liu model is consistently larger than the Lin model.

For the southern hemisphere the Shue model has a larger variation in location of the magnetopause when compared with Cluster data, as described in section 3.3.3.3. In comparison, the asymmetrical models have a more consistent underestimation of the magnetopause location compared to the Cluster data, suggesting they more closely follow the trend found by Cluster. These two models start with underestimations of 8% and 9% for the Lin and Liu models respectively. They then follow the same path until around 55° where

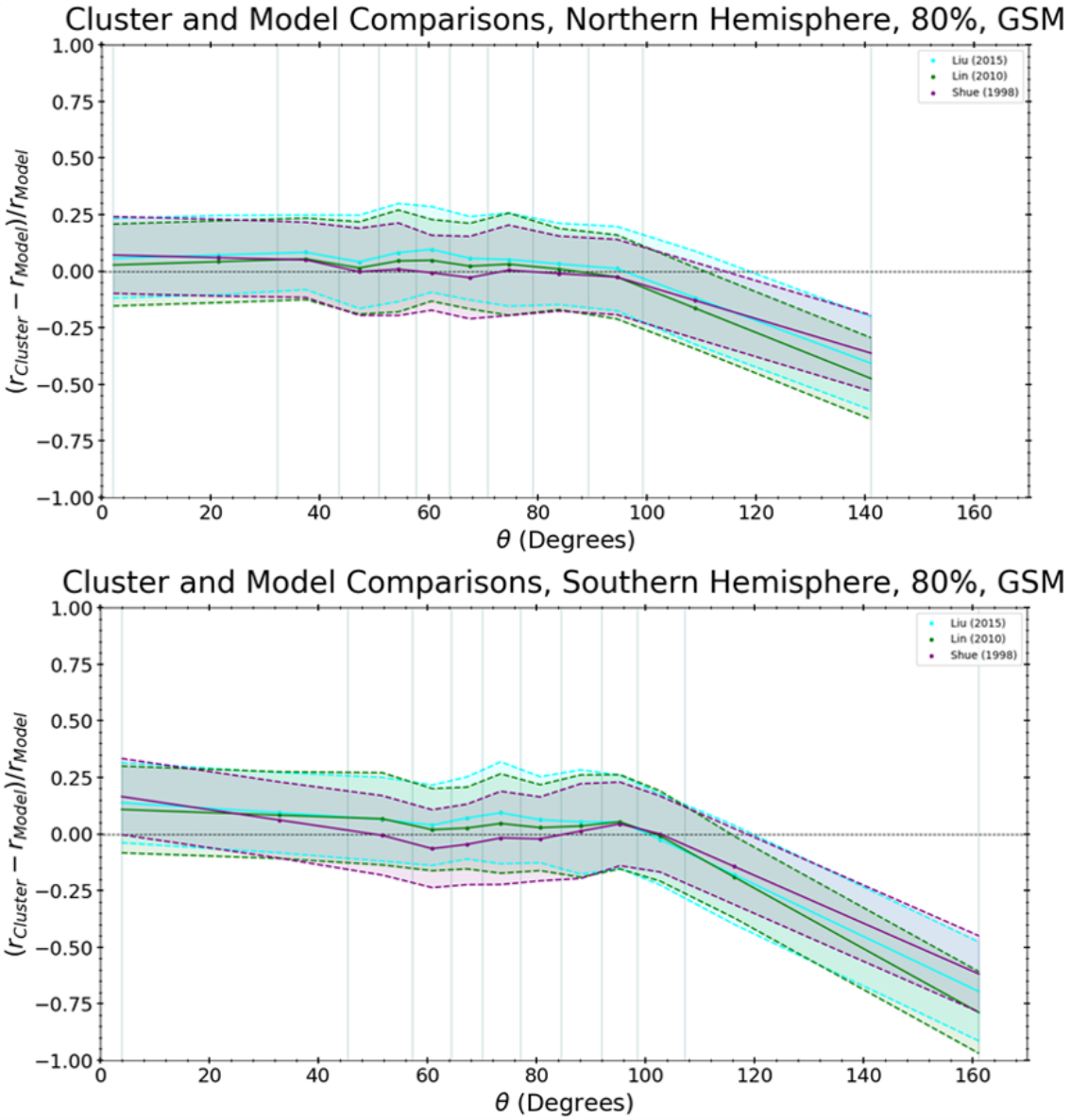

Figure 3.20: Comparison between the Cluster data and all three magnetopause models as angle θ increases. This is for 80% of the crossings in GSM coordinates. The top graph shows the crossings in the northern hemisphere, the bottom graph shows the southern hemisphere

the Liu model underestimates more than the Lin model. This expands to a 5% difference by 73°, before the models seem to merge to a similar path by 90°, before reaching 100°. At around 60°, the Shue model overestimates much more than the asymmetrical models and the Cluster data. This could be the location of the cusp region for the southern hemisphere,

as the Shue model won't account for this region, since it is cylindrically symmetric. In this range of latitudes there seems to be a disagreement between all three models in the southern hemisphere, which would be consistent with the cusp region, as the two asymmetrical models differ in shape for this region. However, this disagrees with the location of the cusp region found in Pitout and Bogdanova (2021) of between latitudes 75° and 80°.

3.5.4 Local Time Variation

For the quadrants created when dividing the local time, figure 3.21 has been created. This is using the same method of calculation as in section 3.3.3.4, similar to what was analysed for figure 3.12. The trends for the asymmetrical models in both of these graphs, local time 0 to 6 and 18 to 24, are relatively similar to the ones produced by the Shue model. This shows there is minimal difference between symmetrical and asymmetrical models beyond 90°. However, between 0 and 6 local time there is between a 3% and 6% difference between the two asymmetrical models, with the Lin model overestimating more than the Liu model. The Shue model more closely follows the trend and extent of overestimation with the Liu model, staying within 3% of this model. For the local time 18 to 24 graph, the Shue and Lin models closely follow an almost identical trend: starting with the largest difference between the two models of 4%, with Lin at a 8% underestimation and Shue at a 4% underestimation. The models then underestimate further, with the Lin model reaching an 11% underestimation by 98°, while the difference between the models reduces to 3%. Both models then start to overestimate more reaching a 5% overestimation of the Shue model by 100°, with the difference between the Shue and Lin model reducing for the rest of the graph. For the Liu model, it follows the same trend as the other two models, within the same proportions until the 100° mark. Beyond this the Liu model significantly overestimates compared to the Cluster data and the other models. Overall, there is more disagreement between the models for the 0 to 6 graph than the 18 to 24 graph. There are a couple of reasons that could cause this, such as the solar wind aberration causing an asymmetry between the dawn side and dusk side of the observed magnetopause. It could be due to slight differences in the models themselves, or how it has been plotted, since the differences may be exaggerated by the extrapolation to the largest θ value. A more detailed study in this area would determine the cause of this effect.

As for the dayside graphs, the Shue model tends to overestimate more than the asymmetrical models, and the Liu model underestimates more than the other two. Looking at the 6 to 12 local time graph, all the models start with a small underestimation compared to the Cluster data. For the Shue model this continues until about 45°, at which it would consistently slightly overestimate. The asymmetrical models slightly underestimate, with the Liu model underestimating further at some points within the 90°. They separate by at most 3%, with the largest underestimation of 7% occurring with the Liu model at 80°. The Shue model disagrees with the asymmetrical models from about 40°, likely due to the lower latitude data

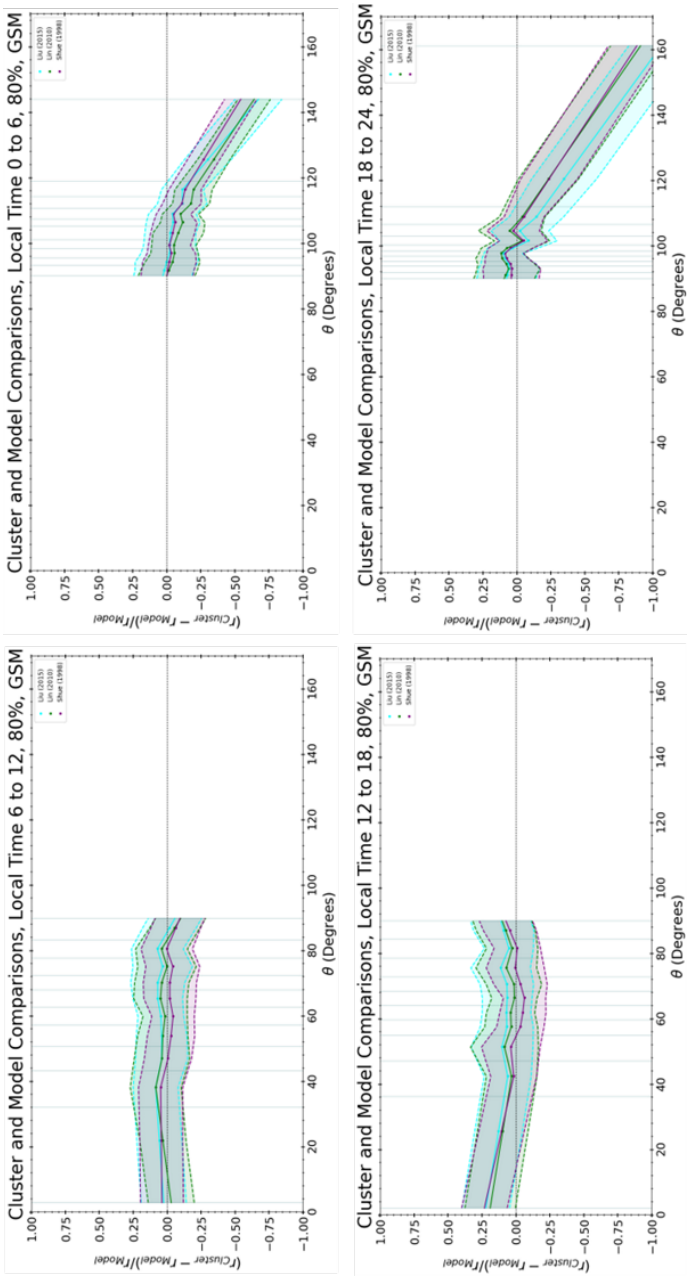

Figure 3.21: Comparison between the Cluster data and all three magnetopause models as angle θ increases. This is for 80% of the crossings in GSM coordinates. The bottom left shows the crossings between local times 6 and 12, the top left shows local times 0 to 6, bottom right shows 12 to 18 and top right shows between 18 and 24

the Shue model is derived from, causing the higher latitude estimations to be less accurate. The difference seen in the Liu model here is likely due to the solar wind aberration; where Liu doesn't account for it within the model, whereas the other two models do account for it.

With the local time 12 to 18 graph, the models start with a larger underestimation of around 10% to 13%. While starting with this noticeable underestimation the Shue model trends towards the Cluster data. The Shue model then agrees with this data except from a section of overestimation between 55° and 75°. This is near the cusp section of the magnetopause, which would cause an overestimation from the Shue model compared to the Cluster data and the asymmetrical models. The asymmetrical models both maintain an underestimation, fluctuating around 6%, with at most a 5% difference between the two models. The solar wind aberration may also cause this difference, due to differences caused between the dawn and dusk sides of the magnetopause, with the Lin model taking this factor into account and the Liu model not. The source of this difference may also be with the formation of the models, since the magnetohydrodynamic simulation (Liu) will likely have differences from a purely empirical model (Lin and Shue), especially when the magnetopause is divided into smaller fragments, such as the local time segments.

Chapter 4

Conclusions and Future Work

This investigation has included the analysis of a new dataset available for the Cluster mission, and the comparison of the Cluster data with various magnetopause models. The GRMB dataset (Grison *et al.*, 2025) allows for easy identification of the region in which the Cluster spacecraft are located at any time, without the need for the user to analyse the field and plasma data directly. This proves a useful resource, but one not without errors. The magnetopause crossings will have a varied length, due to the thickness of the magnetopause, and the approach angle Cluster has with the magnetopause. The GRMB dataset suggests some crossings exceed the expectation of these factors, up to 15 Earth radii for some cases, an effect that can be seen in figure 3.3. This motivated an investigation into the proportion of data that can be trusted (section 3.3.2). By converting the standard deviation found in figure 3.6 to Earth radii and comparing it to a cumulative distribution function of the length of each crossing (figure 3.7), it can be interpreted that 83% of the data can be trusted. With 17% of the longer crossings being identified as untrustworthy boundary determinations; this dataset needs further investigation.

By using the position of magnetopause crossings included in the GRMB dataset, an estimate of the magnetopause location was found. This was then compared to the predicted location of the magnetopause given by the Shue *et al.* (1998) model, a cylindrically symmetric model. This comparison expanded to include asymmetrical models in the form of the Lin *et al.* (2010) and Liu *et al.* (2015) models. This analysis suggests that on average the models underestimate the radial location of the magnetopause compared to the Cluster prediction, over a variety of latitudes and local times. However, there is some agreement between models and the Cluster data, with comparable standard deviations; at most a 15% deviation from the Cluster prediction. The largest difference between the models arises with the magnetospheric cusp region, which can be seen in figure 3.20 in the southern hemisphere at around 55°.

The comparison of magnetopause models to Cluster data includes a significant shift towards

an overestimation of the models at larger θ values (more towards the magnetotail). This may be a result of the sampling bias of Cluster, coming into effect at around 100°. Cluster's orbit will limit the number of magnetopause crossings within this region, as these crossings will only occur in periods of higher magnetosphere compression. This causes less crossings within this region with a bias towards smaller magnetospheres, potentially shifting the comparison towards an overestimation by the models. However, this will come with a more compressed magnetopause surface from the models, diminishing this potential Cluster sampling bias. Furthermore, considerations have to be taken for the models own contribution to this overestimation effect at θ values larger than 100°. The Shue model has been seen to struggle to predict the higher latitude regions compared to the Cluster data and the other models, which could contribute to the overestimation. However, the overestimation is seen with the other models aswell, and to different extents. This suggests it may be a result of the models themselves, with the differences between them causing a varied effect in this region. This would need to be studied further to determine the cause for this overestimation.

Due to the short time-frame this project was undertaken in, there were several aspects which were beyond the scope of this investigation, but could be investigated further in future. One of these aspects is comparing the GRMB dataset to an algorithm based dataset, one in which parameters are set using code to identify magnetopause crossings within magnetic data. This would allow the comparison of the longer magnetopause crossings found within the GRMB dataset to a similar time within the algorithm based dataset, to confirm whether they are correct identifications. This would also allow the identification of any possible errors through the misidentification of the magnetopause regions as other regions of the magnetosphere, and to identify if a manually constructed dataset or an algorithm dataset has higher accuracy and precision.

Investigating the true cause of both the underestimation at the nose of the magnetopause, and the overestimation at θ values larger than 100°, would also be highly valuable to the understanding of the models and GRMB dataset. This would correct for a number of uncertain conclusions throughout this analysis.

Further analysis could have gone into the structure of the magnetopause: the thickness, and the current pattern. This could have been achieved with Cluster by utilising the tetrahedral formation of the four spacecraft. This allows measurements of the magnetopause to be taken within seconds of each other, allowing slight changes in the structure to be identified, requiring the analysis of the raw Cluster data. With more time on this project, utilisation of Cluster in this way is very much possible.

Bibliography

Ariane 501 Inquiry Board Report (1996). URL: https://esamultimedia.esa.int/docs/esa-x-1819eng.pdf.

Berchem, J. and et al. (1998). "The distant tail at 200 RE: Comparison between Geotail observations and the results from a global magnetohydrodynamic simulation". In: *JOURNAL OF GEOPHYSICAL RESEARCH-SPACE PHYSICS*. DOI: 10.1029/97JA02926.

Berchem, Jean and C. T. Russell (1982). "The thickness of the magnetopause current layer: ISEE 1 and 2 observations". In: *Journal of Geophysical Research: Space Physics* 87.A4, pp. 2108–2114. DOI: 10.1029/JA087iA04p02108.

Bianco, Stefano, Bernhard Haas, and Yuri Y. Shprits (2023). "PINE-RT: An operational real-time plasmasphere model". In: *Frontiers in Astronomy and Space Sciences* Volume 10 - 2023. ISSN: 2296-987X. DOI: 10.3389/fspas.2023.1116396.

Borovsky, Joseph E. et al. (2020). "Outstanding questions in magnetospheric plasma physics: The pollenzo view". In: *Journal of Atmospheric and Solar-Terrestrial Physics* 208, p. 105377. ISSN: 1364-6826. DOI: 10.1016/j.jastp.2020.105377.

Cahill, L. J. and P. G. Amazeen (1963). "The boundary of the geomagnetic field". In: *Journal of Geophysical Research (1896-1977)* 68.7, pp. 1835–1843. DOI: 10.1029/JZ068i007p01835.

Cargill, P. J. et al. (2005). "Cluster at the Magnetospheric Cusps". In: *Space Science Reviews*. DOI: 10.1007/s11214-005-3835-0.

Chandran, Benjamin Divakar Giles et al. (2025). "A two-fluid solar-wind model with intermittent Alfvénic turbulence". In: *Journal of Plasma Physics* 91.4, E125. DOI: 10.1017/S0022377825100640.

Chapman, S. and V. C. A. Ferraro (1931a). "A new theory of magnetic storms". In: *Terrestrial Magnetism and Atmospheric Electricity* 36.2, pp. 77–97. DOI: 10.1029/TE036i002p00077.

— (1931b). "A new theory of magnetic storms". In: *Terrestrial Magnetism and Atmospheric Electricity* 36.3, pp. 171–186. DOI: 10.1029/TE036i003p00171.

— (1933). "A new theory of magnetic storms". In: *Terrestrial Magnetism and Atmospheric Electricity* 38.2, pp. 79–96. DOI: 10.1029/TE038i002p00079.

Cornish, Neil J. (1998). *The Lagrange Points*. URL: https://science.nasa.gov/wp-content/uploads/2023/07/3322_lagrange.pdf.

Credland, J. and et al. (1997). "THE CLUSTER MISSION: ESA'S SPACEFLEET TO THE MAGNETOSPHERE". In: *Space Science Reviews*. DOI: 10.1023/A:1004914822769.

De Keyser, J., M. W. Dunlop, C. J. Owen, B. U. Ö Sonnerup, et al. (2005a). "Magnetopause and Boundary Layer". In: *Space Science Reviews*. DOI: 10.1007/s11214-005-3834-1.

— (2005b). "Magnetopause and Boundary Layer". In: *Outer Magnetospheric Boundaries: Cluster Results*. Ed. by G. Paschmann et al. Dordrecht: Springer Netherlands, pp. 231–320. ISBN: 978-1-4020-4582-0. DOI: 10.1007/1-4020-4582-4_9. URL: https://doi.org/10.1007/1-4020-4582-4_9.

Dunlop, M. W. et al. (1999). "Dawnside magnetopause observed by the Equator-S Magnetic Field Experiment: Identification and survey of crossings". In: *Journal of Geophysical Research: Space Physics* 104.A8, pp. 17491–17497. DOI: 10.1029/1999JA900214.

Eggington, J. W. B. et al. (2020). "Dipole Tilt Effect on Magnetopause Reconnection and the Steady-State Magnetosphere-Ionosphere System: Global MHD Simulations". In: *Journal of Geophysical Research: Space Physics* 125.7, e2019JA027510. DOI: 10.1029/2019JA027510.

ESA (2007). *Earth's Magnetic Environment*. URL: https://sci.esa.int/web/cluster/-/41918-earth-s-magnetic-environment.

— (2015). *Cluster II operations*. URL: https://www.esa.int/Enabling_Support/Operations/Cluster_II_operations.

— (2024). *Goodnight, Cluster: brilliant end to trailblazing mission*. URL: https://www.esa.int/Science_Exploration/Space_Science/Cluster/Goodnight_Cluster_brilliant_end_to_trailblazing_mission.

— (n.d.[a]). *Cluster Overview*. URL: https://www.esa.int/Science_Exploration/Space_Science/Cluster/Cluster_overview.

— (n.d.[b]). *Instruments I*. URL: https://www.esa.int/Science_Exploration/Space_Science/Cluster/Instruments_I_Wave_Experiment_Consortium?1.

— (n.d.[c]). *Instruments II*. URL: https://www.esa.int/Science_Exploration/Space_Science/Cluster/Instruments_II.

Escoubet, C. P. et al. (2021). "Cluster After 20 Years of Operations: Science Highlights and Technical Challenges". In: *Journal of Geophysical Research: Space Physics* 126.8, e2021JA029474. DOI: 10.1029/2021JA029474.

Fairfield, Donald H. (1971). "Average and unusual locations of the Earth's magnetopause and bow shock". In: *Journal of Geophysical Research (1896-1977)* 76.28, pp. 6700–6716. DOI: 10.1029/JA076i028p06700.

Ferradas, C. P. et al. (2023). "The effects of particle injections on the ring current development during the 7-8 September 2017 geomagnetic storm". In: *Frontiers in Astronomy and Space Sciences* Volume 10 - 2023. ISSN: 2296-987X. DOI: 10.3389/fspas.2023.1278820.

Förster, M. and S. Haaland (2015). "Interhemispheric differences in ionospheric convection: Cluster EDI observations revisited". In: *Journal of Geophysical Research: Space Physics* 120.7, pp. 5805–5823. DOI: 10.1002/2014JA020774.

Ganushkina, N. Yu., M. W. Liemohn, and S. Dubyagin (2018). "Current Systems in the Earth's Magnetosphere". In: *Reviews of Geophysics* 56.2, pp. 309–332. DOI: 10.1002/2017RG000590.

Grison, Benjamin and et al. (2025). "Localization of the Cluster satellites in the geospace environment". In: *Scientific Data*. DOI: 10.1038/s41597-025-04639-z.

Hands, A. D. P. et al. (2018). "Radiation Effects on Satellites During Extreme Space Weather Events". In: *Space Weather* 16.9, pp. 1216–1226. DOI: 10.1029/2018SW001913.

Hedgecock, P. C. and B. T. Thomas (June 1975). "HEOS Observations of the Configuration of the Magnetosphere". In: *Geophysical Journal International* 41.3, pp. 391–403. DOI: 10.1111/j.1365-246X.1975.tb01622.x.

Hill, T. W. (1974). "Origin of the plasma sheet". In: *Reviews of Geophysics* 12.3, pp. 379–388. DOI: 10.1029/RG012i003p00379.

King, Joe and Natalia Papitashvili (n.d.). *One min and 5-min solar wind data sets at the Earth's bow shock nose*. URL: https://omniweb.gsfc.nasa.gov/html/HROdocum.html.

Laundal, K. M. and A. D. Richmond (2017). "Magnetic Coordinate Systems". In: *Space Science Reviews*. DOI: 10.1007/s11214-016-0275-y.

Lin, R. L. et al. (2010). "A three-dimensional asymmetric magnetopause model". In: *Journal of Geophysical Research: Space Physics* 115.A4. DOI: 10.1029/2009JA014235.

Lin, RuiLin and et al. (2010). "Comparison of a new model with previous models for the low-latitude magnetopause size and shape". In: *Chinese Science Bulletin*. DOI: 10.1007/s11434-009-0533-4.

Liu, Z.-Q. et al. (2015). "A three-dimensional high Mach number asymmetric magnetopause model from global MHD simulation". In: *Journal of Geophysical Research: Space Physics* 120.7, pp. 5645–5666. DOI: 10.1002/2014JA020961.

Lucek, E. A. et al. (2005). "The Magnetosheath". In: *Outer Magnetospheric Boundaries: Cluster Results*. Ed. by G. Paschmann et al. Dordrecht: Springer Netherlands, pp. 95–152. ISBN: 978-1-4020-4582-0. DOI: 10.1007/1-4020-4582-4_4. URL: https://doi.org/10.1007/1-4020-4582-4_4.

Merka, J. et al. (2005). "Three-dimensional position and shape of the bow shock and their variation with upstream Mach numbers and interplanetary magnetic field orientation". In: *Journal of Geophysical Research: Space Physics* 110.A4. DOI: 10.1029/2004JA010944.

NASA (n.d.[a]). *Cluster-II*. URL: https://science.nasa.gov/mission/cluster/.

— (n.d.[b]). *Satellite Situation Center Web*. URL: https://sscweb.gsfc.nasa.gov/cgi-bin/Locator_graphics.cgi.

Olson, W. P. (1969). "The shape of the tilted magnetopause". In: *Journal of Geophysical Research (1896-1977)* 74.24, pp. 5642–5651. DOI: 10.1029/JA074i024p05642.

Owens, Mathew J. and Robert J. Forsyth (2013). "The Heliospheric Magnetic Field". In: *Living Reviews in Solar Physics*. DOI: 10.12942/lrsp-2013-5.

Paschmann, G. et al. (1979). "Plasma acceleration at the Earth's magnetopause: evidence for reconnection". In: *Nature*. DOI: 10.1038/282243a0.

Pitout, F. and Y. V. Bogdanova (2021a). "The Polar Cusp Seen by Cluster". In: *Journal of Geophysical Research: Space Physics* 126.9, e2021JA029582. DOI: 10.1029/2021JA029582.

— (2021b). "The Polar Cusp Seen by Cluster". In: *Journal of Geophysical Research: Space Physics* 126.9, e2021JA029582. DOI: 10.1029/2021JA029582.

Roelof, Edmond C. and David G. Sibeck (1993). "Magnetopause shape as a bivariate function of interplanetary magnetic field Bz and solar wind dynamic pressure". In: *Journal of Geophysical Research: Space Physics* 98.A12, pp. 21421–21450. DOI: 10.1029/93JA02362.

Shue, J.-H., J. K. Chao, et al. (1997). "A new functional form to study the solar wind control of the magnetopause size and shape". In: *Journal of Geophysical Research: Space Physics* 102.A5, pp. 9497–9511. DOI: 10.1029/97JA00196.

Shue, J.-H., P. Song, et al. (1998). "Magnetopause location under extreme solar wind conditions". In: *Journal of Geophysical Research: Space Physics* 103.A8, pp. 17691–17700. DOI: 10.1029/98JA01103.

Sibeck, D. G., R. E.Lopez, and E. C.Roelof (1991). "Solar wind control of the magnetopause shape, location, and motion". In: *Journal of Geophysical Research: Space Physics* 96.A4, pp. 5489–5495. DOI: 10.1029/90JA02464.

Sibeck, D. G. and R.-Q. Lin (2014). "Size and shape of the distant magnetotail". In: *Journal of Geophysical Research: Space Physics* 119.2, pp. 1028–1043. DOI: 10.1002/2013JA019471.

Van Doorsselaere, Tom et al. (2020). "Coronal Heating by MHD Waves". In: *Space Science Reviews*. DOI: 10.1007/s11214-020-00770-y.

Wang, Chih-Ping, Larry R. Lyons, and Vassilis Angelopoulos (2014). "Properties of low-latitude mantle plasma in the Earth's magnetotail: ARTEMIS observations and global MHD predictions". In: *Journal of Geophysical Research: Space Physics* 119.9, pp. 7264–7280. DOI: 10.1002/2014JA020060.